Heliyon 9 (2023) e20320

Contents lists available at ScienceDirect

Heliyon

journal homepage: www.cell.com/heliyon

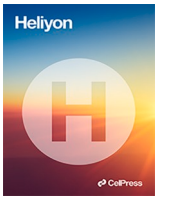

Evaluating the skills of the CMIP5 global climate models using multicriteria decision-making analysis in Ethiopia

Endalkachew Tesfaye [a,*], Brook Abate [b], Taye Alemayehu [a], Yihun Dile [c]

[a] Ethiopian Institute of Water Resources, Addis Ababa University, Addis Ababa, Ethiopia
[b] College of Architecture & Civil Engineering, Addis Ababa Science & Technology University, Addis Ababa, Ethiopia
[c] College of Agriculture & Life Sciences, Texas A & M University, College Station, TX, USA

ARTICLE INFO

Keywords:
Precipitation
Temperature
GCM
Multimodel ensemble
Multicriteria decision-making

ABSTRACT

This study evaluates the skills of 30 CMIP5 GCMs and the Multimodel Ensemble (MME) in reproducing the characteristics of observed precipitation (Pr), minimum (T_{min}), and maximum (T_{max}) temperature over the Middle Awash sub-basin (MASB) in Ethiopia. The MME of the climate variables was generated using the simple arithmetic mean method. The entire analysis was performed on the raw historical GCM simulations (before bias correction) and observed data for the periods 1981–2005 based on monthly and annual time series data over the annual and seasonal temporal resolutions. This study considered two approaches. The first one was an evaluation of GCMs employing five statistical performance metrics (SPMs), i.e., mean, CV, PBIAS, RSR, and r. The second approach involves the application of multicriteria decision-making (MCDM) analysis, adopting three SPMs (PBIAS, RSR, and r). The relative weights of the three metrics were determined by the entropy method. Besides, the weighted average and compromise programming techniques were employed to rank and select the best-performing GCMs. The findings from the first approach using five SPMs demonstrate that, for a given variable of interest, a GCM that performs well for one SPM may fail to produce the same for another SPM on the same temporal scale. Likewise, for the same SPM at different resolutions, a GCM may perform well for a one-time scale but poorly for another. These suggested that the results of GCM skills relied mainly on the SPM, time scale, and data formats chosen for analysis. Hence, it is critical to comprehensively evaluate the skill of GCMs using multiple performance metrics over a range of spatial and temporal settings and data formats. In addition, results of the MCDM analysis proved that the ensemble of GCMs, which provide adequate performance in simulating the salient features of Pr, T_{min}, and T_{max} concomitantly across the MASB, encompass CMCC-CMS, BCC-CSM1.1(m), CMCC-CM, BNU-ESM, CanESM2, and MPI-ESM-MR. However, it was observed that different GCMs performed much differently in characterizing various variables over a range of temporal scales and data formats. The MME also proved its superior potential in duplicating the climate of the study area over several individual GCMs. The overall findings attested that instead of aggregating the ranks from the three variables into one, it is recommended to treat each variable independently while developing a subset of best-performing GCMs for ensembling since each GCM responds differently to each variable under a set of conditions. Finally, the approaches and findings from this study will be valuable input for subsequent climate and hydrologic studies in the study area and beyond.

* Corresponding author.
E-mail addresses: endalkachew.tesfaye@aau.edu.et, endalktesf1221@gmail.com (E. Tesfaye).

https://doi.org/10.1016/j.heliyon.2023.e20320
Received 6 April 2023; Received in revised form 18 September 2023; Accepted 19 September 2023
Available online 20 September 2023

1. Introduction

Precipitation and temperature are among the decisive climate variables while studying the effects of climate change on multiple sectors [1]. Climate change-induced alterations in the patterns of precipitation and temperature cause variations in the hydrological cycle and ecological system, apart from their impact on socioeconomic development and human health [2]. Research made so far has verified increases in the severity and frequency of droughts [3], floods [4], and heat waves [5], and decreases in the severity and frequency of cold snaps [6] in recent years, which are signs of abrupt variations in the precipitation and temperature regimes. Therefore, climate change has been posing severe challenges for humans that considerably threaten their existence and development. Thus, climate change impact assessments have been conducted through simulations of precipitation and temperature, and the measures for climate change impacts have appeared to be significant [2].

The study of past, current, and future climate variability and trends has been made possible with the help of valuable tools called global climate models (GCMs) [7,8]. GCMs are 3-D numerical models operating on the principles of fluid dynamics, thermodynamics, and radiative heat transfer that have been capable of simulating and predicting past, current, and future climate in response to diverse emission scenarios [9]. Also, GCMs represent various atmospheric processes of the global climate system, and they are the primary tools for estimating future climate patterns and studying variations in precipitation and temperature patterns [10]. GCMs are mainly developed to simulate and project climate on a global scale [11]. To date, many GCMs have been crafted and used for the simulation and projection of the Earth's climate.

However, uncertainties in developing and applying GCMs like initial and boundary conditions, representation of the atmospheric and other processes in the GCMs, parameter and model structures, imperfect conceptualizations, parameterization schemes, calibration procedures and data, pertinent assumptions, emission scenarios, spatial resolution, and so on significantly affect their output [11–13]. Hence, all GCMs cannot be used directly to project future climate effects for a particular area. To reduce the uncertainty related to the GCMs, a limited number of GCMs should be chosen to get rid of those models that do not match the climate of the selected area [14].

The Intergovernmental Panel on Climate Change (IPCC) brought the Coupled Model Intercomparison Project Phase 5 (CMIP5) through the World Climate Research Program (WCRP), with a set of GCMs available from various institutions, to complete the preparation of the Fifth Assessment Report (AR5) [15]. The CMIP5 models showed considerable improvements in climate simulations, in contrast with its previous generation of CMIP3 GCMs [16–19]. Currently, above 50 GCMs are available in the CMIP5 collection with different model characteristics and spatial resolutions [20]. However, human and computational resources pose a restriction on the size of the subset of GCMs used in a climate change impact assessment [21]. Hence, evaluation and ranking of suitable GCMs or a set of GCMs before their selection are very crucial in climate change impact studies given the large number of available GCMs. In addition, the selection of credible GCMs is considered one of the effective ways to reduce uncertainty in climate change projections [22–24].

The choice of a climate model can vary depending on the purpose and future projections. Different approaches could be adopted for model selection, such as (a) taking all the models or ensembles with available data and simply calculating the mean of all predicted outcomes [25], (b) using a past performance approach, which relies on the capability of GCMs to reproduce past climates without taking future forecasts into account [26,27], (c) the envelope approach, which selects GCMs based on their agreement with future climate projections without considering the GCMs potential to replicate the past climate [28], (d) the hybrid approach, combines the envelope approach with the past performance approach [29,30] and takes past performance and future climate projections of GCMs into account, and e) the multicriteria decision-making approaches [23,31].

Different studies have attempted to evaluate the ability of the CMIP5 GCMs and CORDEX Africa RCMs in simulating precipitation and temperature at the global scale [2,9,10,13,14,17,21,22,24,26,28,30], regional scale [23,29,32–38], and sub-regional (national) scale [39–46]. So far, the multimodel ensembles of the CMIP5 GCMs for the projection of climate variables have been effectively used [47], and some authors have confirmed the superiority of these ensembles over individual GCMs [48]. However, other studies have suggested that multimodel ensembles are deficient in their projection [49,50], and thus it may be essential to consider acceptable GCMs for specific assessments rather than simple multimodel ensembles [51]. Further investigations have suggested various ensemble methods to be used for the best-performing GCMs [52]. Hence, assessing the skill of GCMs would also provide valuable information for future climate change studies on the application of multimodel ensembles.

Given the above discussion, the following research gaps were identified: (a) none of the available investigations were able to holistically assess the performance of several CMIP5 GCMs, in simulating both precipitation and temperature, at various temporal resolutions over the Middle Awash sub-basin (MASB) except for [41] which evaluated 24 CMIP5 GCMs in Northwest Ethiopia and the entire Awash basin based on the annual cycle, seasonal bias, trend, and variability; (b) available studies lack the benefit of multiple statistical performance metrics (SPMs) to evaluate the skill of models, in simulating both precipitation and temperature, and hence to rank and select the best GCMs in the sub-basin; and (c) the application of MCDM analysis to evaluate, rank, and select a suitable GCM or a subset of GCMs was totally missing in the MASB.

Therefore, the primary aim of this study is to comprehensively assess the skill of 30 CMIP5 GCMs, including the MME, in simulating historical precipitation, minimum, and maximum temperatures under various temporal scales over the MASB. The Multimodel Ensemble (MME) or ensemble mean of the simulations from 30 GCMs was also computed and compared with individual GCMs in the evaluation process to identify and confirm any added value that is achieved by the combination of individual GCMs. Observed precipitation and temperature datasets for the 1981–2005 baseline periods were considered for the evaluation. Moreover, three SPMs, i.e., correlation coefficient (r), ratio of Root Mean Square Error (RMSE) to the standard deviation of observed data (RSR), and Percent of Bias (PBIAS) were used to evaluate the skill of GCMs with MCDM analysis techniques.

The findings from this study will answer which of the CMIP5 GCMs adequately represents the observed precipitation and temperature over the MASB during the reference period. The outputs will also help guide modeling institutions to refine subsequent model developments through the identification of the weaknesses and strengths of the models evaluated as part of this study. Besides, it will assist researchers interested in extending investigations for future climate and hydrologic modeling studies in the MASB.

The remaining sections of this paper are organized and presented as follows: Section two describes the study area, data sources, datasets employed, and materials and methods adopted, whereas the third section provides the findings, followed by the discussion and recommendations in the fourth section. The fifth section highlights the conclusion part.

2. Materials and methods

2.1. Description of the study area

One of Ethiopia's important river basins is the Awash River Basin (ARB). It starts in the Central Ethiopian Highlands and moves northeast until emptying into Lake Abe. The river has a total length of over 1200 km and a drainage area of close to 114,000 km^2 [53]. The three distinct zones of the ARB are the Upper, Middle, and Lower Awash sub-basins [54]. The Middle Awash sub-basin (MASB) is found in the middle part of the ARB between the Upper and Lower Awash sub-basins. It is geographically located between latitudes of 8°36′52.4'' - 10°48′8.0″ N and longitudes of 39°42′46.4'' - 41°36′0.6″ E (Fig. 1). The total sub-basin area is estimated at 30,882.3 km^2. The altitude of the MASB ranges from 462 to 3670 m above mean sea level (amsl), with an average elevation of 1061 m amsl.

Extreme variations in temperature and precipitation characterize the ARB, which stretches from cold mountainous parts to semi-desert regions. The magnitude and timing of precipitation (Pr) and the movement of the Intertropical Convergence Zone (ITCZ) produced three distinct seasons in the MASB [55]. These are Kiremt (summer), Bega (winter), and Belg (autumn), with Kiremt being the major wet season (June–September), Bega being the dry season (October–January), and Belg being the minor rainy season (February–May). Hence, the Pr was classified as having a bimodal pattern (Fig. 2). Besides, the average annual Pr varies from 1646 mm in the elevated areas to 430 mm in the lowland parts, with a mean annual Pr of 695 mm in the sub-basin (Table 1). In the same way, the average annual minimum (T_{min}), mean (T_{mean}), and maximum (T_{max}) temperatures of the sub-basin are 17.4 °C, 25.5 °C, and 33.5 °C, respectively (Fig. 2).

2.2. Data sources

The input data for this study includes observed meteorological data, historical GCM simulations, and the Digital Elevation Model (DEM) of the sub-basin. As described below, the data was gathered from a variety of sources.

2.2.1. Observed data

Initially, the National Meteorological Agency (NMA) of Ethiopia provided historical observed climate data (1981–2015) for 49 stations in and surrounding the MASB. The data was often marked by a broad range of data lengths (1–34 years) and missing values (5–96%), at least for the key meteorological variables (Pr, T_{min}, and T_{max}). The majority of these data had record lengths that were too short (often less than 15 years) with too many missing values (generally greater than 10%), making them unfit for climate and environmental studies and analysis. Hence, high-resolution (4 km) spatially and temporally complete gridded historical climate data (precipitation and temperature) were received from the NMA on a daily temporal resolution over the 1981–2015 periods. The gridded dataset was developed by blending the available observed and proxy datasets, both from satellite and reanalysis products. The International Research Institute (IRI) for Climate and Society at Columbia University provided considerable support for the NMA in the development of the gridded data through its Enhancing National Climate Services (ENACTS) initiative [56]. Table 1 shows the summary of precipitation and temperature data extracted from the gridded datasets for seventeen (17) climate stations in the study area.

The selection of stations was triggered by data length, percent of missing values, availability of at least 3 important climate variables (Pr, T_{min}, and T_{max}), recently observed data for grid (merged) data validation, and also to ensure a fair distribution of stations in the sub-basin. For a better understanding, the term "observed" in the subsequent sections of the paper was utilized to mean the merged (gridded) dataset given the inherent limitations in the observed stations data over the sub-basin.

2.2.2. Global climate models data

The fifth phase of the Coupled Model Intercomparison Project (CMIP5) is a joint effort with the aspiration to improve scientific knowledge related to climate change [9], and it involves 20 climate modeling or research groups around the world with over 40 GCMs. The outputs from CMIP5 contain historical climate simulations (1850–2005) and climate projections for near-term and long-term timeframes with four Representative Concentration Pathways (RCPs).

To evaluate the skill of 30 GCMs, their daily averages of minimum near-surface air temperature (T_{min}), daily averages of maximum near-surface air temperature (T_{max}), and daily surface precipitation (Pr) for the 1981–2005 baseline periods were taken. The atmosphere, ocean, land, and sea surface temperature conditions were taken to initialize historical simulations from these GCMs and forced by observed natural and anthropogenic CO_2 and aerosol concentrations to project future outputs [57]. The detailed description of the GCMs considered for this evaluation, coupled with their modeling centers, GCM acronyms, complete model names, spatial resolutions, and the number of ensemble members, is shown in Table 2 below. For each GCM, historical simulations from one ensemble member were considered for the evaluation. Yet, the MMEs of these 30 GCMs were estimated with the simple arithmetic mean method to assess

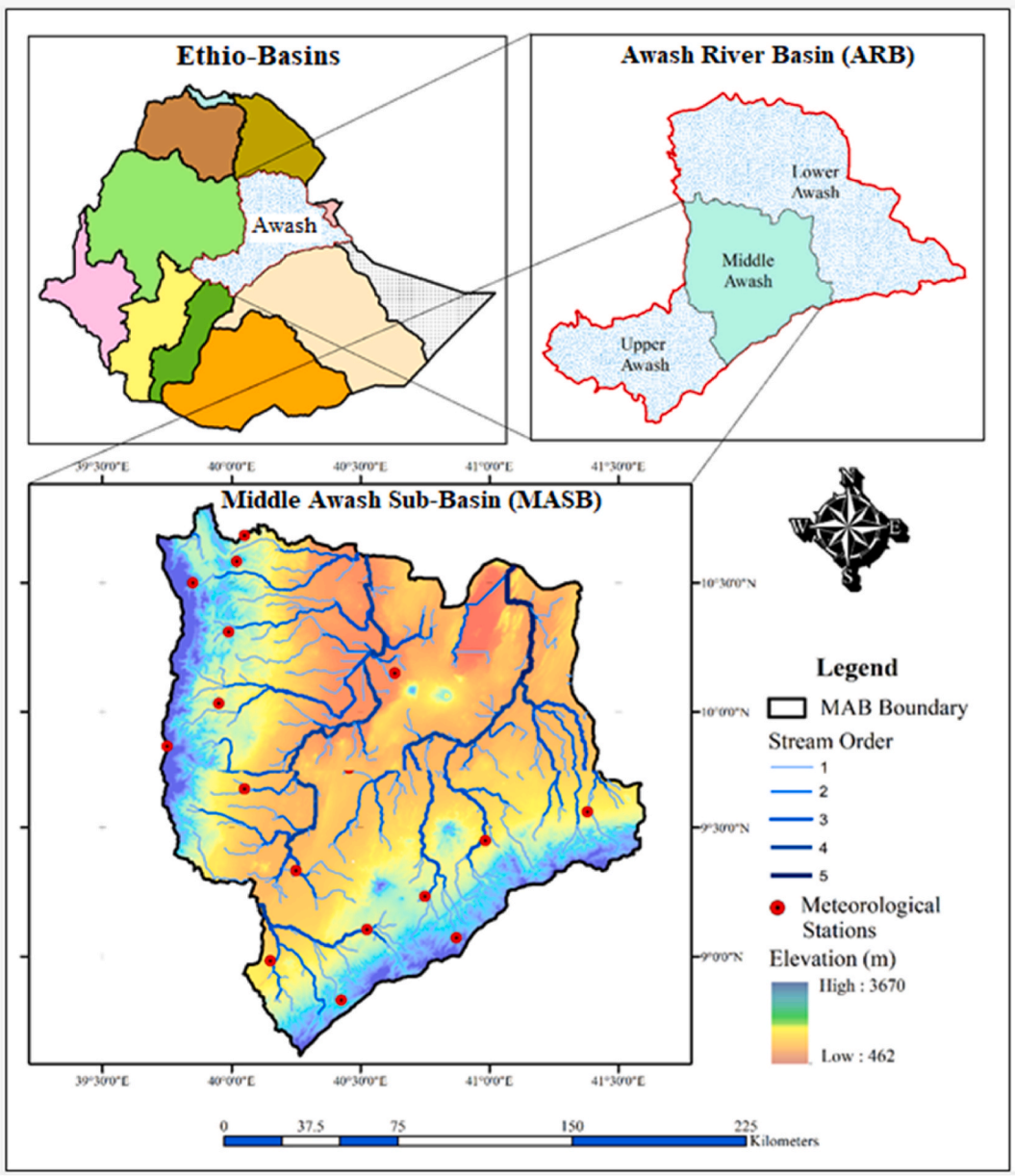

Fig. 1. Location map of the study area[1].

the capability of the MMEs as well.

The 30 GCMs were chosen for evaluation because of the availability of both historical and future climate simulations under the commonly used emission scenarios of RCP 4.5 and RCP 8.5 in the CMIP5 project. Daily Pr, T_{min}, and T_{max} data from these models were captured in Network Common Data Format (NetCDF4) from the Global Earth System Grid Federation (ESGF) web portals, which are accessible to the general public at https://esgf-index1.ceda.ac.uk,

2.3. Methods

2.3.1. Data extraction and quality control process

The location information of meteorological stations was used to extract point data from the gridded dataset received from the NMA

[1] The high-resolution (12.5 × 12.5 m) Radiometric Terrain Corrected (RTM) ALOS PALSAR DEM data was supplied by the Alaska Satellite Facility (ASF), a division of the University of Alaska Fairbanks' Geophysical Institute [[84]].

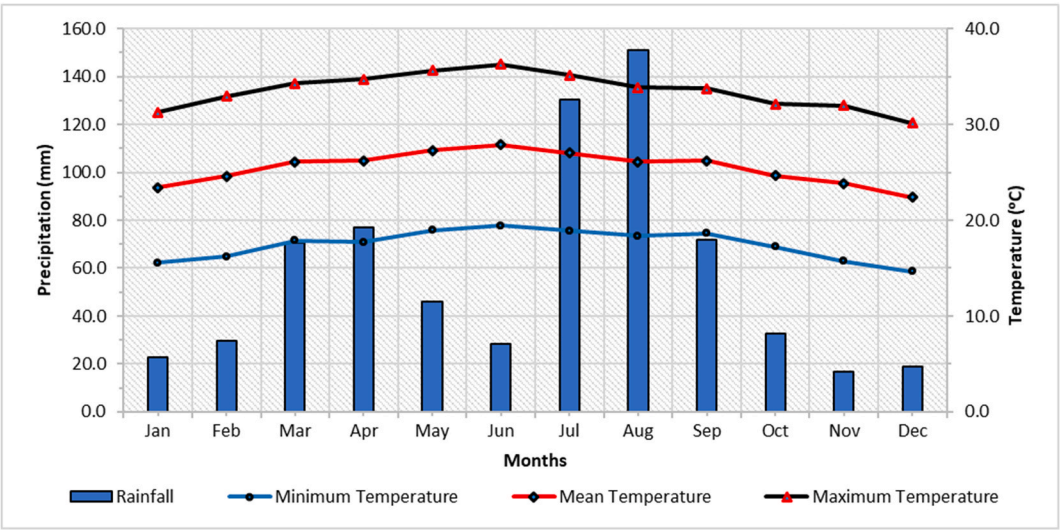

Fig. 2. Mean monthly precipitation and temperature in MASB (1981–2005).

Table 1
Mean annual precipitation and temperature of meteorological stations in the MASB (1981–2005).

No.	Meteorological Stations	Latitude (DD)	Longitude (DD[a])	Elevation (m)	Class	Region	Mean Annual Pr (mm)	Mean Temperature (°C)	Missing Data[b] (%)
1	Abayater	9.65	40.05	862	3	Amhara	883.6	22.9	18.0
2	Afdem	9.45	40.98	1056	3	Somali	638.0	25.8	34.6
3	Artuma	10.58	40.02	1880	3	Amhara	962.3	21.6	27.3
4	Asebe Teferi	9.07	40.87	1792	3	Oromia	888.4	21.4	15.3
5	Awash 7 Kilo	8.98	40.15	923	3	Afar	865.8	25.1	15.7
6	Awash Sheleko	9.33	40.25	737	3	Afar	430.2	28.0	25.1
7	Bora	10.68	40.05	1500	4	Amhara	853.1	22.4	17.7
8	Debre Sina	9.87	39.75	2800	4	Amhara	1645.7	14.2	8.6
9	Efeson	10.03	39.95	1500	3	Amhara	1193.4	22.7	11.5
10	Erer	9.56	41.38	1088	1	Somali	563.3	26.9	49.8
11	Gedamaytu	9.73	40.46	792	3	Afar	445.2	28.1	53.5
12	Gewane	10.15	40.63	568	1	Afar	488.9	29.0	19.2
13	Hardium	8.83	40.43	1649	4	Oromia	967.0	21.6	64.7
14	Jara	10.31	39.99	1960	4	Amhara	1005.4	21.9	6.1
15	Kora	9.10	40.53	1530	4	Oromia	655.2	24.6	18.1
16	Majete	10.50	39.85	2000	1	Amhara	889.8	20.9	5.1
17	Mieso Aviation	9.23	40.75	1400	1	Oromia	577.2	23.6	10.5

[a] DD means Degree Decimal.
[b] Percent of missing data for precipitation.

of Ethiopia. However, by contrasting the extracted historical climate data with the corresponding observed data at each station, the trustworthiness of the gridded data was validated. The Pr, T_{min}, and T_{max} data were considered satisfactory in most of the stations, with coefficients of determination (R) and correlation coefficient (r) values above 0.64 and 0.80, respectively. Additionally, utilizing the stations' location data and the nearest neighbor interpolation technique, the Pr, T_{min}, and T_{max} data from each GCM were extracted using a Python script.

Through the use of algorithms and techniques detailed in the programs – (OutlierFlag [58] and XLSTAT 2018 [59]), the quality of the data, the treatment of outliers, and the verification of the homogeneity of the data values were assessed. The validity and dependability of the data can be verified using homogeneity tests. Four techniques (Petitt, Standard Normal Homogeneity Test (SNHT), Buishand, and von Neumann) were used in this investigation to confirm the homogeneity of the data [59]. These methods have been used to demonstrate that a series is homogeneous throughout a specific period. After being verified, the inhomogeneous series were corrected appropriately, and then they were made homogeneous by adjusting them statistically according to the instructions provided in the AnClim software [60].

2.3.2. Areal precipitation and temperature analyses

The point-observed data from each station was converted into spatial data with the Thiessen polygon method [61] using ArcGIS 10.8 software. This method was utilized to partition the study area into smaller areas (polygons) based on the area of influence of the

Table 2
Detailed description of GCMs considered in this study.

Modeling Center (Group) Acronym	Modeling Center (Group), Country	GCM Acronym	GCM Name	Atmospheric Horizontal Resolution (lon x lat)	Number of Ensemble Members
CSIRO-BOM	Commonwealth Scientific and Industrial Research Organization and Bureau of Meteorology, **Australia**	ACCESS1.0	Australian Community Climate and Earth-System Simulator version 1.0	1.88° × 1.25°	2
CSIRO-BOM	Commonwealth Scientific and Industrial Research Organization and Bureau of Meteorology, **Australia**	ACCESS1.3	Australian Community Climate and Earth-System Simulator version 1.3	1.88° × 1.25°	3
BCC	Beijing Climate Center, China Meteorological Administration, **China**	BCC-CSM1.1 (m)	Beijing Climate Center - Climate System Model version 1.1(m)	1.12° × 1.12°	3
BCC	Beijing Climate Center, China Meteorological Administration, **China**	BCC-CSM1.1	Beijing Climate Center - Climate System Model version 1.1	2.8° × 2.8°	3
GCESS-BNU	College of Global Change and Earth System Science, Beijing Normal University, **China**	BNU-ESM	Beijing Normal University - Earth System Model	2.8° × 2.8°	1
CCCma	Canadian Center for Climate Modeling and Analysis, **Canada**	CanESM2	Canadian Earth System Model - second generation	2.8° × 2.8°	5
NCAR	National Center for Atmospheric Research, **USA**	CCSM4	Community Climate System Model version 4	1.25° × 0.94°	6
NSF-DOE-NCAR	National Science Foundation, Department of Energy, National Center for Atmospheric Research, **USA**	CESM1-BGC	Community Earth System Model - Biogeochemical Model	1.25° × 0.94°	1
NSF-DOE-NCAR	National Science Foundation, Department of Energy, National Center for Atmospheric Research, **USA**	CESM1-CAM5	Community Earth System Model - Community Atmosphere Model version 5	1.25° × 0.94°	3
CMCC	Centro Euro-Mediterraneo sui Cambiamenti Climatici, **Italy**	CMCC-CM	Centro Euro-Mediterraneo sui Cambiamenti Climatici -Climate Model	0.75° × 0.75°	1
CMCC	Centro Euro-Mediterraneo sui Cambiamenti Climatici, **Italy**	CMCC-CMS	Centro Euro-Mediterraneo sui Cambiamenti Climatici -Climate Model with a resolved Stratosphere	1.88° × 1.87°	1
CNRM-CERFACS	Centre National de Recherches Meteorologiques/Centre Europeen de Recherche et Formation Avancees en Calcul Scientifique, **France**	CNRM-CM5	National Center of Meteorological Research – Coupled Model version 5	1.4° × 1.4°	10
CSIRO-QCCCE	Commonwealth Scientific and Industrial Research Organization, Queensland Climate Change Centre of Excellence, **Australia**	CSIRO-Mk3-6-0	Commonwealth Scientific and Industrial Research Organization – Mark version 3.6.0	1.8° × 1.8°	10
ICHEC	EC-EARTH consortium published at Irish Centre for High-End Computing, **Netherlands/Ireland**	EC-EARTH	European Consortium – Earth system model	1.13° × 1.12°	14
LASG-CESS	Institute of Atmospheric Physics, Chinese Academy of Sciences, **China;** and CESS, Tsinghua University	FGOALS-g2	Flexible Global Ocean-Atmosphere-Land System Model - Grid-point version 2	2.8° × 2.8°	5
NOAA-GFDL	Geophysical Fluid Dynamics Laboratory, **USA**	GFDL-CM3	Geophysical Fluid Dynamics Laboratory - Coupled Model version 3	2.5° × 2.0°	5
NOAA-GFDL	Geophysical Fluid Dynamics Laboratory, **USA**	GFDL-ESM2G	Geophysical Fluid Dynamics Laboratory - Earth System Model version 2G	2.5° × 2.0°	1
NOAA-GFDL	Geophysical Fluid Dynamics Laboratory, **USA**	GFDL-ESM2M	Geophysical Fluid Dynamics Laboratory - Earth System Model version 2 M	2.5° × 2.0°	1
MOHC	Met Office Hadley Centre, **UK**	HadGEM2-CC	Hadley Center Global Environment Model version 2 – Carbon Cycle model	1.88° × 1.25°	3
MOHC	Met Office Hadley Centre, **UK**	HadGEM2-ES	Hadley Center Global Environment Model version 2 – Earth System model	1.88° × 1.25°	4
INM	Russian Academy of Sciences, Institute of Numerical Mathematics, **Russia**	INMCM4.0	Institute for Numerical Mathematics Coupled Model version 4.0	2.0° × 1.5°	1
IPSL	Institut Pierre Simon Laplace, **France**	IPSL-CM5A-LR	Institut Pierre Simon Laplace – Climate Model version 5A – Low Resolution	3.75° × 1.8°	6
IPSL	Institut Pierre Simon Laplace, **France**	IPSL-CM5A-MR	Institut Pierre Simon Laplace – Climate Model version 5A – Medium Resolution	2.5° × 1.25°	3

(*continued on next page*)

Table 2 (*continued*)

Modeling Center (Group) Acronym	Modeling Center (Group), Country	GCM Acronym	GCM Name	Atmospheric Horizontal Resolution (lon x lat)	Number of Ensemble Members
MIROC	Atmosphere and Ocean Research Institute (The University of Tokyo), National Institute for Environmental Studies, and Japan Agency for Marine-Earth Science and Technology, **Japan**	MIROC5	Model for Interdisciplinary Research on Climate version 5	1.4° × 1.4°	1
MIROC	Atmosphere and Ocean Research Institute (The University of Tokyo), National Institute for Environmental Studies, and Japan Agency for Marine-Earth Science and Technology, **Japan**	MIROC5-ESM	Model for Interdisciplinary Research on Climate version 5 – Earth System Model	2.8° × 2.8°	3
MIROC	Atmosphere and Ocean Research Institute (The University of Tokyo), National Institute for Environmental Studies, and Japan Agency for Marine-Earth Science and Technology, **Japan**	MIROC5-ESM-CHEM	Model for Interdisciplinary Research on Climate version 5 - Earth System Model - An atmospheric Chemistry coupled version	2.8° × 2.8°	3
MPI-M	Max Planck Institute for Meteorology, **Germany**	MPI-ESM-LR	Max Planck Institute - Earth System Model – Low Resolution	1.88° × 1.87°	3
MPI-M	Max Planck Institute for Meteorology, **Germany**	MPI-ESM-MR	Max Planck Institute - Earth System Model – Medium Resolution	1.88° × 1.87°	3
MRI	Meteorological Research Institute, **Japan**	MRI-CGCM3	Meteorological Research Institute – Coupled Global Climate Model version 3	1.1° × 1.1°	5
NCC, NMI	Bjerknes Centre for Climate Research, Norwegian Meteorological Institute, **Norway**	NorESM1-M	Norwegian Climate Center's Earth System Model - core version	2.5° × 1.9°	3

stations to calculate areal Pr, T_{min}, and T_{max}. The method calculates areal values for each polygon based on the area of the polygon in proportion to the total area of the sub-basin. Similarly, the Thiessen polygon method was considered to determine the areal Pr, T_{min}, and T_{max} of each GCM and the MME in the MASB [62]. After the observed, GCMs and the MME data were changed into areal average (spatial) data, different SPMs were employed to assess the GCMs' skill in simulating the characteristics of Pr, T_{min}, and T_{max} in the sub-basin.

2.3.3. *Performance evaluation of climate models*

Prominently, two approaches were followed to measure the skill of models at simulating the characteristics of the three variables in the sub-basin. The first approach considers the evaluation of GCMs using five statistical metrics, including mean, coefficient of variation (CV), percentage of bias (PBIAS), ratio of root mean square error to the standard deviation of observed data (RSR), and Pearson correlation coefficient (r).

An analysis of the variability of annual and seasonal Pr, T_{min}, and T_{max} data about the mean was conducted utilizing the CV. It is obtained by dividing the standard deviation by the mean. A larger CV value indicates more variable data, with values less than 20% attesting to low variability, between 20% and 30% attesting to moderate variability, and values over 30% attesting to high variability in the series [63].

PBIAS is the deviation of the data being evaluated, expressed as a percentage, and used to measure the difference between GCM simulations and observed data. A PBIAS close to 0 attests to a minor systematic difference between observed data and GCM simulations, whereas a PBIAS far away from 0 indicates a deviation. It could be positive or negative. A positive value signals an overestimation of model bias, and the reverse is true for negative values [62].

$$\mathrm{PBIAS} = \frac{\sum_{i=1}^{N}\left(X_i^{GCM} - X_i^{Obs}\right)}{\sum_{i=1}^{N} X_i^{Obs}} \mathrm{x}100 \quad [1]$$

The advantages of error index statistics are incorporated into RSR, and a scaling or normalizing factor is also included so that the resulting statistic and reported values can be extended to a variety of constituents. RSR ranges from a big positive value to an ideal value of 0, which represents zero residual variation, or RMSE, and hence a perfect model simulation. The quality of the model simulation improves with decreasing RSR and RMSE [62].

$$RSR = \frac{RMSE}{STDEV_{Obs}} = \frac{\left[\sum_{i=1}^{N}\left(X_i^{GCM} - X_i^{Obs}\right)^2\right]}{\left[\sum_{i=1}^{N}\left(X_i^{GCM} - X^{\overline{Obs}}\right)^2\right]} \quad [2]$$

The correlation is usually utilized to evaluate the linear relationship between the GCM simulation and the observed area-averaged values. Values close to 1.0 signal a better relationship among the variables, and a value away from 1.0 demonstrates less agreement [62].

$$r = \frac{\sum_{i=1}^{N}\left(X_i^{GCM} - X^{\overline{GCM}}\right)\left(X_i^{Obs} - X^{\overline{Obs}}\right)}{\sqrt{\sum_{i=1}^{N}\left(X_i^{GCM} - X^{\overline{GCM}}\right)^2}\sqrt{\sum_{i=1}^{N}\left(X_i^{Obs} - X^{\overline{Obs}}\right)^2}} \quad [3]$$

where X_i^{GCM} is the Pr, T_{min}, and T_{max} of a given GCM at time step i, X_i^{Obs} is the observed Pr, T_{min}, and T_{max} of the sub-basin at time step i, the bar over the variables denotes the average over a period of 1981–2005, and N represents the number of data values over the analysis period.

The second method involves the use of MCDM analysis to measure the performance of models at replicating the observed Pr, T_{min}, and T_{max}. This study would employ two MCDM techniques, i.e., weighted average (WA) and compromise programming (CP). These methods will enable one to rank all the GCMs and identify the best GCMs on the basis of three SPMs (PBIAS, RSR, and r) at a sub-basin scale. Below is a detailed presentation of the MCDM analysis and selected approaches.

2.3.4. Ranking of climate models with multicriteria decision-making (MCDM) tools

MCDM can be perceived as a process of evaluating real-world situations based on various qualitative or quantitative criteria in certain or uncertain environments to suggest a suitable course of action or choice among the available alternatives (models). The problem will become more complex with multiple conflicting and non-commensurable criteria, different units of measurement among the criteria, the presence of quite different alternatives, and the involvement of a range of decision-makers [64]. In this performance assessment, the concept of MCDM was applied to rank all GCMs and select the most suitable models, among others, based on SPMs (criteria) having conflicting and non-commensurable characters. The following sections are devoted to presenting formal procedures to rank and choose the most suitable (best) models.

A) Data Transformation

Since the evaluation criteria proposed in this study have distinct characters and units of measurement, the requirement for data transformation was compulsory before normalization [64]. Hence, PBIAS, which is normally expressed in percentages and receives either positive or negative values, should be transformed into decimal numbers, divided by 100, and positive values, taking absolute values of the figures, given that signs are only direction indicators, i.e., underestimation or overestimation of model biases. Similarly, r, which could either be positive, zero, or negative, should also be converted following the same above approach. Besides, no transformation is required for RSR, given that it has either zero or non-negative decimal values.

B) Data Normalization Approaches

By normalizing the values of the different options available for a specific criterion, the range of values for the criteria with various units can be made to fall between 0 and 1. This procedure also aids in preventing the dominance of the criterion with the larger value over the criterion with the smaller value [64]. Pomerol and Romero [65] proposed four normalizing techniques with distinguishing characteristics. The approach employed in this evaluation is illustrated in Eq. (4) below, and it was chosen based on the facts at hand and the planning issue under discussion.

If $f_j(a)$ is the value of criterion j for alternative (model) a, then the normalized value of criterion j for alternative (model) a, $V_j(a)$, is defined as:

$$v_j(a) = \frac{f_j(a)}{\sum_{a=1}^{m} f_j(a)} \quad [4]$$

where m represents the set or number of alternatives (models).

C) Methods for Estimation of Weights

Numerous methods have been recommended in different studies to estimate the weights assigned to each criterion. Rating, entropy, the Analytic Hierarchy Process (AHP), fuzzy AHP, and revised Simos methods are among the approaches that are broadly used in different professions and applications [65–72]. The entropy method, which is independent of the views of the decision maker and is typically useful for exploring contrasts between sets of data, was adopted for this study [64,69].

Entropy is a term that measures the uncertainty linked with random phenomena of the expected information content of a certain message, and a discrete probability distribution represents this uncertainty [68]. The entropy method estimates the weights of the different criteria from the payoff matrix, a matrix comprising the alternatives (GCMs) and the criteria (SPMs) for evaluation. The philosophy of the method relies on the amount of information available, which can be measured by its entropy and its relationship with

the relevance of the criterion. Pomerol and Romero [65] and Aomar [68] explained the method in the following steps:

(1) For the given normalized payoff matrix, p_{ij}, entropy E_j of the set of alternatives (models) for criterion j is:

$$E_j = -\frac{1}{\ln(m)} \sum_{i=1}^{m} p_{ij} \ln(p_{ij}) \text{ for } j = 1, 2, \ldots J \quad [5]$$

where m is the number of alternatives (models) and j is the number of criterion.

(2) Degree of diversification of the information provided by the outcomes of criterion j is:

$$D_j = 1 - E_j \text{ for } j = 1, 2, \ldots J \quad [6]$$

(3) Normalized weights of the criterion are:

$$w_j = \frac{D_j}{\sum_{j=1}^{J} D_j} \text{ for } j = 1, 2, \ldots J \quad [7]$$

If the entropy value is high, the uncertainty contained in the criterion vector is high, the diversification of the information is low, and correspondingly, the criterion is less important. This method is valuable as it reduces the burden on the decision-maker for large problems. Likewise, the contribution of the decision-maker is limited when estimating the weights of the criteria [64].

D) Approaches for Ranking of GCMs

The methodological approach for ranking and choosing the best (most suitable) alternatives from a group of options was developed by Duckstein [73]. The problem must be defined and the criteria fixed before the collection of any pertinent data. The next crucial steps are the development of viable alternatives and the creation of a payoff matrix (alternatives versus criteria arrays). The choice of an appropriate approach to the problem and the inclusion of the decision-maker's preference structure are the other steps to the final one. Choosing the most suitable or best alternative or alternatives is the last phase for further investigation.

Various MCDM methods are available to rank and select the most suitable among the given non-dominated models. These methods were classified into four groups, i.e., distance, outranking, priority or utility, and mixed type [65,74,75]. Given the diversity of methods under each group, this study adopted only two approaches, i.e., one from the priority- or utility-based method called weighted average (WA) and the other from the distance-based method called compromise programming (CP).

1) Weighted Average (WA) Method

WA is a utility-type MCDM method. It is expressed as the average of the weighted sum of criterion values, i.e.,

$$U_a = w_1 u_1 + w_2 u_2 + w_3 u_3 + \ldots + w_j u_j \quad [8]$$

where U_a is the overall utility value for alternative (model) a; w_1, w_2, w_3, …, w_j are the weights assigned to the criterion; and u_1, u_2, u_3, …, u_j are the corresponding criteria values.

The alternative whose total utility is highest can be regarded as the best. Where appropriate, a suitable normalization procedure should be implemented [64]. In this method, we should multiply the criteria with values of a minimization nature by −1 to allow for a uniform analysis of the subject from a maximization perspective, i.e., (−1*min) = max [51].

Since PBIAS and RSR are criteria that imply the magnitude of biases and errors in the GCMs, they have a minimization nature; i.e., GCMs with minimum values of PBIAS and RSR are relatively best regardless of the ± signs. However, r has a maximization nature, i.e., GCMs with positive r values are comparatively better than those with negative r values because models positively correlated with the observed data are much better than the others. Towards this end, negative values of PBIAS and RSR from the transformed payoff matrix and actual calculated values of r were considered when estimating U_a in the WA method.

2) Compromise Programming (CP) Method

CP defines the best (most suitable) solution as the one in the set of efficient solutions whose point is at the least distance from an ideal point [76]. The objective is to get a solution that is as 'close" as possible to some "ideal" solution. The distance measure used in CP is from the family of L_p-metrics and is expressed as:

$$L_p(a) = \left[\sum_{j=1}^{J} w_j^p \left| f_j^* - f_j(a) \right|^p \right]^{1/p} \quad [9]$$

If the criteria are not expressed in commensurable terms, a suitable normalization approach can be incorporated to ensure a similar range for each criterion, i.e., [0, 1]. With this note, Eq. (9) transforms to:

$$L_p(\mathrm{a}) = \left[\sum_{\mathrm{j}=1}^{J} w_j^p \left|\frac{f_\mathrm{j}^* - f_\mathrm{j}(a)}{M_j - m_j}\right|^p\right]^{1/p} \quad [10]$$

where $L_p(a) = L_p$-metric for alternative (model) a, $f_j(a)$ = value of criterion j for alternative a, M_j = maximum value of criterion j in the set N, m_j = minimum value of criterion j in the set N, f_j^* = ideal value of criterion j, w_j = weight assigned to the criterion j, and p = parameter or balancing factor reflecting the interest of the decision-maker with regard to compensation between deviations.

For p = 1, all deviations from fj* are considered in direct proportion to their magnitudes. For p = 2, the largest deviation is the only one taken into account, corresponding to zero compensation between deviations [64]. A value of p = 1 was taken for this study. Like the WA method, the computation of L_p in the CP technique involves negative values of PBIAS and RSR from the transformed payoff

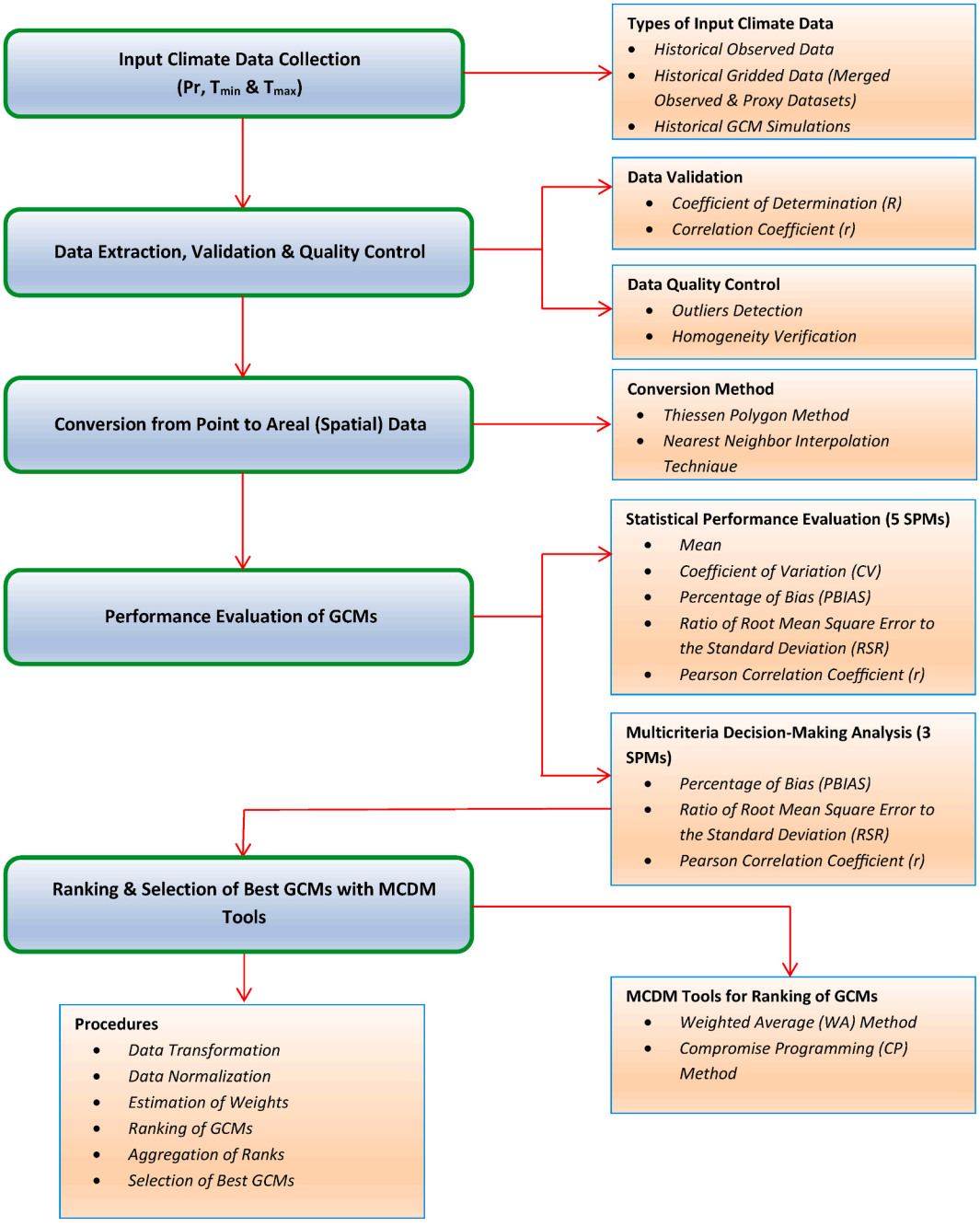

Fig. 3. A diagram showing the whole flow chart of the work.

matrix and actual calculated values of r from the original matrix.

E) Aggregation of Ranks

Following the establishment of ranks for each GCM, including the MME, with the above techniques over a set of temporal scales, using Monthly Time Series (MTS) and Annual Time Series (ATS) data, the best models that adequately reproduce the observed climatology were ranked and selected following the below simple approach to aggregate the ranks from each analysis:

i) Sum up the ranks for each model, including the MME, acquired from the two methods under various temporal resolutions with the MTS and ATS data;
ii) The GCMs and the MME with the highest sum of ranks become the worst, and those with the lowest sum become the best (most suitable) models among the existing alternatives.

Fig. 3 below diagrammatically depicts the entire workflow of the project, including the datasets gathered, methodology, and approaches used while carrying out this study.

3. Results

3.1. Statistical performance evaluation of GCMs

3.1.1. Mean annual and seasonal climate characteristics

(a) Mean precipitation

The mean annual Pr in the sub-basin, based on ATS data, was relatively better captured by the MME, MPI-ESM-MR, HadGEM2-ES,

Table 3
Mean annual Pr, T_{min} and T_{max} of GCMs, MME and observed data over the MASB based on ATS data (1981–2005).

No	GCMs	Mean Annual Pr (mm)				Mean Annual T_{min} (°C)				Mean Annual T_{max} (°C)			
		Annual	JJAS	FMAM	ONDJ	Annual	JJAS	FMAM	ONDJ	Annual	JJAS	FMAM	ONDJ
1	ACCESS1.0	908.3	559.9	208.6	139.8	14.3	17.3	13.9	11.7	27.2	26.8	29.2	25.4
2	ACCESS1.3	848.3	633.1	120.0	95.2	15.2	18.2	14.7	12.7	25.8	26.7	27.5	23.3
3	BCC-CSM1.1(m)	549.0	304.3	153.9	90.7	16.2	19.0	15.7	14.0	29.2	31.6	29.8	26.1
4	BCC-CSM1.1	871.8	446.9	303.0	121.9	16.6	16.9	17.5	15.3	26.9	25.5	28.7	26.5
5	BNU-ESM	859.1	651.3	107.1	100.7	15.9	18.0	16.2	13.5	27.3	26.7	29.8	25.5
6	CanESM2	522.4	381.4	103.3	37.7	12.2	17.5	11.7	7.4	32.2	31.1	34.2	31.3
7	CCSM4	867.6	580.4	103.0	184.2	14.9	17.9	14.3	12.5	25.4	26.1	28.0	22.2
8	CESM1-BGC	851.0	590.5	120.2	140.3	15.1	18.0	14.6	12.6	25.8	26.2	28.4	22.7
9	CESM1-CAM5	1005.8	679.5	168.3	157.9	14.9	17.7	14.8	12.4	24.9	24.1	27.7	23.0
10	CMCC-CM	348.4	110.0	131.7	106.6	16.3	21.7	17.7	14.8	30.0	33.3	30.0	26.6
11	CMCC-CMS	578.7	277.0	153.6	148.1	17.5	20.9	17.0	14.6	29.2	31.7	29.7	26.3
12	CNRM-CM5	464.0	317.8	99.8	46.4	10.4	14.1	10.2	7.0	33.2	34.1	35.3	30.1
13	CSIRO-Mk3-6-0	418.9	139.2	211.7	68.0	14.8	19.0	13.7	11.8	29.3	32.9	29.1	26.0
14	EC-EARTH	614.2	384.4	176.6	53.2	15.0	17.6	15.1	12.3	25.8	26.0	26.9	24.6
15	FGOALS-g2	1272.5	906.9	138.3	127.4	14.7	15.1	15.9	13.1	24.4	22.5	26.7	23.9
16	GFDL-CM3	583.7	336.9	89.3	157.5	15.6	19.4	16.1	11.4	27.7	29.4	29.7	23.9
17	GFDL-ESM2G	505.9	225.0	121.6	159.3	18.4	20.8	18.9	15.4	27.0	28.2	29.1	23.6
18	GFDL-ESM2M	513.3	247.5	108.9	156.9	18.7	21.2	19.3	15.8	27.4	28.7	29.4	24.0
19	HadGEM2-CC	781.8	538.7	158.3	84.8	12.3	15.7	11.7	9.6	26.9	26.2	29.2	25.1
20	HadGEM2-ES	754.9	547.3	142.8	64.7	12.8	16.2	12.2	9.9	27.1	26.4	29.5	25.5
21	INMCM4.0	757.8	535.3	75.7	146.8	7.7	15.9	3.7	3.4	27.5	28.1	30.0	24.4
22	IPSL-CM5A-LR	36.2	21.3	5.0	9.9	11.3	15.9	9.8	8.2	28.8	32.1	29.1	25.2
23	IPSL-CM5A-MR	185.4	133.6	19.7	32.1	13.2	16.2	12.7	10.5	28.5	30.9	29.0	25.6
24	MIROC5	1329.7	611.8	468.4	249.5	17.1	19.1	17.2	15.0	27.4	28.8	27.7	25.8
25	MIROC5-ESM	1270.4	827.4	240.8	202.2	15.3	16.6	16.3	13.1	24.1	23.4	27.4	21.3
26	MIROC5-ESM-CHEM	1248.1	839.0	220.2	188.9	15.4	16.7	16.3	13.2	24.2	23.4	27.6	21.4
27	MPI-ESM-LR	466.8	296.1	116.4	54.3	11.3	15.9	9.8	8.2	28.5	30.4	29.4	25.7
28	MPI-ESM-MR	646.6	404.1	173.9	68.6	13.2	16.2	12.7	10.5	27.9	29.5	28.8	25.5
29	MRI-CGCM3	250.6	54.9	103.1	92.8	16.2	19.9	15.8	12.9	30.8	34.7	31.1	26.6
30	NorESM1-M	807.7	504.5	119.2	184.0	14.5	16.2	14.9	12.4	23.8	22.7	26.7	21.9
31	MME	704.0	436.2	152.1	115.7	14.6	17.7	14.3	11.8	27.5	28.3	29.2	25.0
32	**Observed**	**695.0**	**381.2**	**222.8**	**90.9**	**17.4**	**18.8**	**17.7**	**15.8**	**33.5**	**34.7**	**34.4**	**31.4**

Note: Values typed with red and blue font colors demonstrate overestimation and underestimation of the observed mean values, correspondingly. However, the best (minimum departures from the observed mean values) and the worst (considerable departures from the observed mean values) five GCMs from each were shaded with bright green and yellow colors, respectively, for quick identification in the table.

INMCM4.0, and EC-EARTH consecutively. These GCMs demonstrate minimal relative deviations against the observed Pr. Among the five, three models (MME, HadGEM2-ES, and INMCM4.0) overestimated the Pr, and the other two (MPI-ESM-MR and EC-EARTH) underestimated it. Conversely, MIROC5-ESM-CHEM, MIROC5-ESM, FGOALS-g2, MIROC5, and IPSL-CM5A-LR are the worst GCMs, in their order of appearance, with considerable departures from the observed Pr (Tables 3 and 4). Four models overestimated the observed Pr except for IPSL-CM5A-LR, which displayed a much lower simulation (Table 3). The ranks of the best and worst GCMs, both for the annual (Jan–Dec) and seasonal temporal scales, are illustrated in Table 4 below.

Similar results for the three variables (Pr, T_{min}, and T_{max}) according to MTS data under various temporal resolutions are also provided in the appendix for further reference (Tables A1 and A2).

(b) Mean minimum and maximum temperature

The top-ranked five models that were comparatively good at representing the mean annual T_{min} over the MASB, again with the smallest relative deviations, are CMCC-CMS, MIROC5, CMCC-CM, BCC-CSM1.1, and GFDL-ESM2G. Except for two models, i.e., MIROC5 and BCC-CSM1.1, the other GCMs overestimated the simulated T_{min} in the sub-basin. Conversely, CanESM2, IPSL-CM5A-LR, MPI-ESM-LR, CNRM-CM5, and INMCM4.0, successively, were the worst GCMs, which were unable to duplicate the T_{min} with substantial departures from the observed values (Tables 3 and 4). The observed T_{min} was underestimated by the five models over the study area. The ranking of the best and worst GCMs over the four temporal resolutions is presented in Table 4 below.

Like precipitation, the MME was not a member of the worst GCMs over the four temporal scales, which suggests its superior advantage over many other individual GCMs. Besides, the average observed T_{min} over the four temporal scales was underestimated by most GCMs except for CMCC-CMS, CMCC-CM, GFDL-ESM2G, BCC-CSM1.1(m), CSIRO-Mk3-6-0, MIROC5, GFDL-CM3, and GFDL-ESM2M.

Considering the annual temporal scale, the best-performing models for T_{max} comprise CNRM-CM5, CanESM2, MRI-CGCM3, CMCC-CM, and CSIRO-Mk3-6-0. They have better skills in capturing the mean observed T_{max} in the sub-basin (Table 4). The departures, in contrast to the worst GCMs, are minimal (Table 3). However, CESM1-CAM5, FGOALS-g2, MIROC5-ESM-CHEM, MIROC5-ESM, and NorESM1-M are the least performing models, among others, which show sizable discrepancies from the observed mean value. Surprisingly, all the GCMs in Table 4 underestimated the T_{max} in the MASB. Table 4 also provides the ranks of the best and worst models over the annual and seasonal time scales. Here also, the MME was not among the worst GCMs over the four temporal resolutions, which shows its superior benefit over the other individual GCMs.

Table 4
Rank of best and worst GCMs for Pr, T_{min} and T_{max} over the annual and seasonal temporal scales based on ATS data.

Annual (Jan-Dec) Temporal Scale												
No.	Mean Pr				Mean T_{min}				Mean T_{max}			
	Best GCMs	Rank	Worst GCMs	Rank	Best GCMs	Rank	Worst GCMs	Rank	Best GCMs	Rank	Worst GCMs	Rank
1	MME	1	MIROC5-ESM-CHEM	27	CMCC-CMS	1	CanESM2	27	CNRM-CM5	1	CESM1-CAM5	27
2	MPI-ESM-MR	2	MIROC5-ESM	28	MIROC5	2	IPSL-CM5A-LR	28	CanESM2	2	FGOALS-g2	28
3	HadGEM2-ES	3	FGOALS-g2	29	CMCC-CM	3	MPI-ESM-LR	28	MRI-CGCM3	3	MIROC5-ESM-CHEM	29
4	INMCM4.0	4	MIROC5	30	BCC-CSM1.1	4	CNRM-CM5	30	CMCC-CM	4	MIROC5-ESM	30
5	EC-EARTH	5	IPSL-CM5A-LR	31	GFDL-ESM2G	5	INMCM4.0	31	CSIRO-Mk3-6-0	5	NorESM1-M	31
JJAS Temporal Scale (Major Rainy Season - Kiremt)												
No.	Mean Pr				Mean T_{min}				Mean T_{max}			
	Best GCMs	Rank	Worst GCMs	Rank	Best GCMs	Rank	Worst GCMs	Rank	Best GCMs	Rank	Worst GCMs	Rank
1	CanESM2	1	MRI-CGCM3	27	BCC-CSM1.1(m)	1	IPSL-CM5A-LR	27	MRI-CGCM3	1	CESM1-CAM5	27
2	EC-EARTH	2	IPSL-CM5A-LR	28	CSIRO-Mk3-6-0	2	MPI-ESM-LR	27	CNRM-CM5	2	MIROC5-ESM	28
3	MPI-ESM-MR	3	MIROC5-ESM	29	MIROC5	3	HadGEM2-CC	29	CMCC-CM	3	MIROC5-ESM-CHEM	28
4	GFDL-CM3	4	MIROC5-ESM-CHEM	30	ACCESS1.3	4	FGOALS-g2	30	CSIRO-Mk3-6-0	4	NorESM1-M	30
5	MME	5	FGOALS-g2	31	GFDL-CM3	4	CNRM-CM5	31	IPSL-CM5A-LR	5	FGOALS-g2	31
FMAM Temporal Scale (Minor Rainy Season - Belg)												
No.	Mean Pr				Mean T_{min}				Mean T_{max}			
	Best GCMs	Rank	Worst GCMs	Rank	Best GCMs	Rank	Worst GCMs	Rank	Best GCMs	Rank	Worst GCMs	Rank
1	MIROC5-ESM-CHEM	1	GFDL-CM3	27	CMCC-CM	1	HadGEM2-CC	27	CanESM2	1	ACCESS1.3	27
2	CSIRO-Mk3-6-0	2	INMCM4.0	28	BCC-CSM1.1	2	CNRM-CM5	28	CNRM-CM5	2	MIROC5-ESM	27
3	ACCESS1.0	3	IPSL-CM5A-MR	29	MIROC5	3	IPSL-CM5A-LR	29	MRI-CGCM3	3	EC-EARTH	29
4	FGOALS-g2	4	IPSL-CM5A-LR	30	CMCC-CMS	4	MPI-ESM-LR	29	CMCC-CM	4	FGOALS-g2	30
5	MIROC5-ESM	5	MIROC5	31	GFDL-ESM2G	5	INMCM4.0	31	INMCM4.0	4	NorESM1-M	31
ONDJ Temporal Scale (Dry Season - Bega)												
No.	Mean Pr				Mean T_{min}				Mean T_{max}			
	Best GCMs	Rank	Worst GCMs	Rank	Best GCMs	Rank	Worst GCMs	Rank	Best GCMs	Rank	Worst GCMs	Rank
1	BCC-CSM1.1(m)	1	NorESM1-M	27	GFDL-ESM2M	1	IPSL-CM5A-LR	27	CanESM2	1	CESM1-BGC	27
2	MRI-CGCM3	2	CCSM4	28	GFDL-ESM2G	2	MPI-ESM-LR	27	CNRM-CM5	2	CCSM4	28
3	ACCESS1.3	3	MIROC5-ESM-CHEM	29	BCC-CSM1.1	3	CanESM2	29	CMCC-CM	3	NorESM1-M	29
4	HadGEM2-CC	4	MIROC5-ESM	30	MIROC5	4	CNRM-CM5	30	MRI-CGCM3	3	MIROC5-ESM-CHEM	30
5	BNU-ESM	5	MIROC5	31	CMCC-CM	5	INMCM4.0	31	BCC-CSM1.1	5	MIROC5-ESM	31

Note: GCMs typed with red font colors represent overestimation and the blue font colors demonstrate underestimation of mean values by the GCMs against the observed data.

3.1.2. Annual and seasonal variability of climate variables

(a) Precipitation

The variability of observed Pr was low for the annual, moderate for the JJAS, and high for the FMAM and ONDJ temporal scales. Also, GCM simulations on the annual time setting demonstrate both low (<20%), moderate (20–30%), and high (>30%) variability over the MASB. Most of the GCMs (16 in number), including the MME, have low variability, with 10 exhibiting moderate variability and the remaining 5 demonstrating high variability in the data (Fig. 4). However, the variability in the IPSL-CM5A-LR (65.7%) is exceptionally high, which makes simulations from this model unreliable in replicating the observed Pr.

Likewise, the CV in the Kiremt season was in the low-to-high range, with 7 GCMs in the high, 5 in the moderate, and the rest 19 in the low variability category. The variability of Pr from the IPSL-CM5A-LR model (102.1%) is again extremely massive, which degrades the dependability of the model (Table 4). On the other side, the CV during the Belg and Bega seasons were in the high class, except for a few models (FGOALS-g2, MIROC5-ESM, and MME for the Belg, and MIROC5-ESM-CHEM and MME for the Bega seasons) (Fig. 4). The variability in the MME data was in the low variability range over the four-time scales, which is a value addition acquired through the ensemble of a subset of GCMs.

(b) Minimum and maximum temperature

The variability of T_{min} and T_{max} over the annual and seasonal time scales for all GCMs, the MME, and the observed temperature is given in Fig. 5 (a, b) below. The observed T_{min} (Fig. 5 (a)) has shown low variability (<20%) across the four temporal scales. Yet, GCM simulations exposed low variability across the four temporal scales except for the INMCM4.0 model, with moderate variability (28.2%) for the Belg and high variability (52.3%) for the Bega seasons. Again, the MME demonstrated low variability across the four periods.

Similarly, the variability of observed T_{max} (Fig. 5 (b)) was low (<20%) over the four-time scales, and the simulated T_{max} variability from the whole GCMs was also in the low variability class, both for the annual and seasonal temporal resolutions. In addition, the variability of T_{max} in the MME was small across the four periods.

3.1.3. PBIAS, r and RSR

(a) Precipitation

The computed values of PBIAS (%), r, and RSR for Pr using Eqs. (1)–(3), respectively, based on MTS data for each model over the four temporal scales, are illustrated in Table 5. The table also provides extra information with different font colors to differentiate the best and least-performing GCMs.

The best models with the smallest PBIAS among the list of GCMs, which considerably reduce model biases, are the MME, MPI-ESM-MR, HadGEM2-ES, INMCM4.0, and EC-EARTH for the annual temporal scale. Conversely, MIROC5-ESM-CHEM, MIROC5-ESM, FGOALS-g2, MIROC5, and IPSL-CM5A-LR were the least suitable models with significant biases over the study area. The best and worst models for the other seasons are also indicated in Table 5 below.

CNRM-CM5, CanESM2, MME, FGOALS-g2, and HadGEM2-ES are the best-performing models with an acceptable degree of a linear

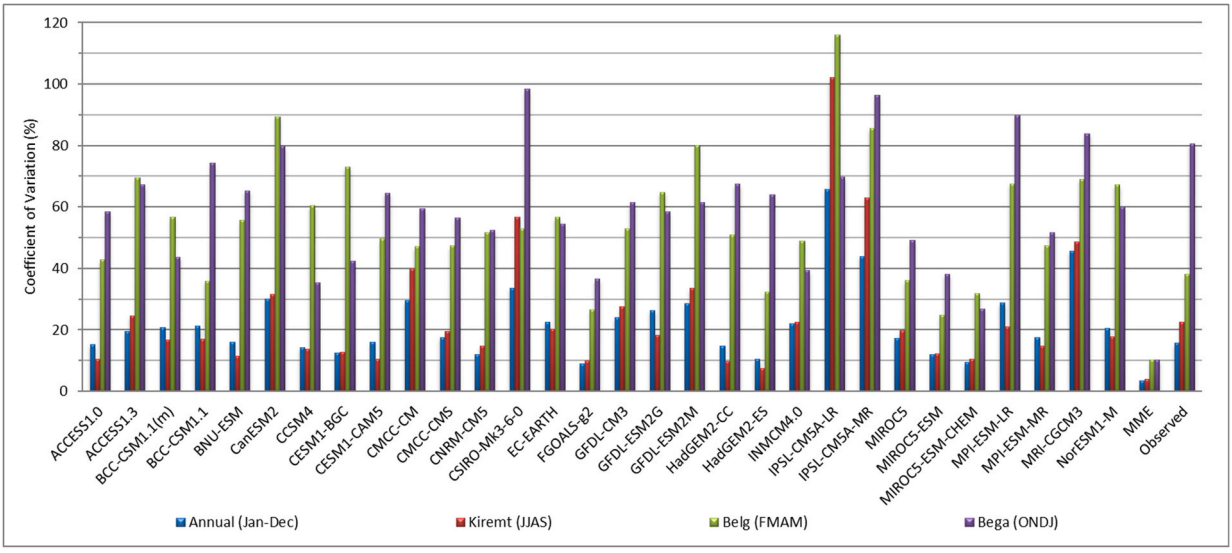

Fig. 4. CV of annual and seasonal precipitation over the MASB.

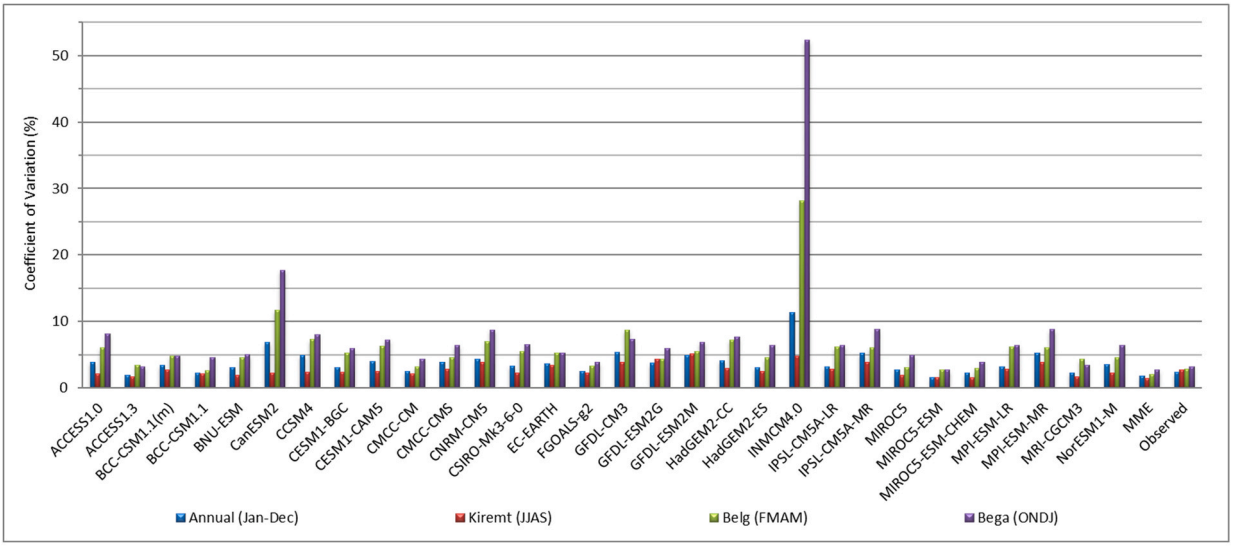

(a) T_{min}

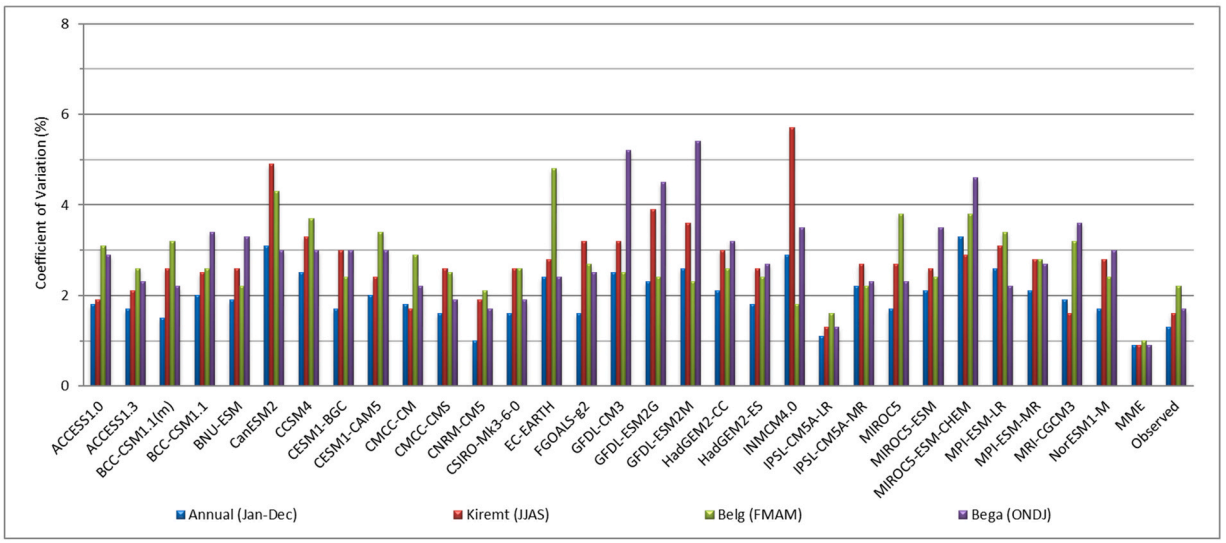

(b) T_{max}

Fig. 5. CV of annual and seasonal T_{min} (a) and T_{max} (b) over the MASB.

relationship among the observed and GCM-simulated Pr. Whereas, the worst GCMs with very weak correlation coefficients were CSIRO-Mk3-6-0, NorESM1-M, CMCC-CM, GFDL-ESM2G, MRI-CGCM3, and GFDL-ESM2M for the same time scale (Table 5). The details for other temporal scales are provided in the same table.

The quality of GCM simulations improves with decreasing RSR. Hence, models with relatively smaller RSR values represent the observed Pr very well and include the MME, CNRM-CM5, CanESM2, BCC-CSM1.1(m), and MPI-ESM-LR for the annual time scale. However, NorESM1-M, MIROC5, MIROC5-ESM-CHEM, FGOALS-g2, and MIROC5-ESM are the worst models with quite a large RSR value in contrast to the others, suggesting their limitations in simulating the sub-basin observed Pr adequately for the same temporal setting. The details for the remaining seasons are also given in Table 5 below. A similar result, according to ATS data, which is not annexed to this manuscript, was also completed for Pr to be employed in the MCDM analysis.

(b) Minimum and maximum temperature

The actual figures of PBIAS, r, and RSR for T_{min} and T_{max} over the four temporal scales are given in the appendix part of this manuscript (Tables B1 and B2). Again, one can simply identify the best and worst models in light of their respective values, marked

Table 5
PBIAS, r and RSR between observed and historical GCM simulations for annual and seasonal Pr over the MASB based on MTS data (1981–2005).

No	GCMs	PBIAS (%)				r (-)				RSR (-)			
		Annual	JJAS	FMAM	ONDJ	Annual	JJAS	FMAM	ONDJ	Annual	JJAS	FMAM	ONDJ
1	ACCESS1.0	30.7	46.9	-6.4	53.7	0.55	0.51	0.04	0.33	1.16	1.23	1.48	1.70
2	ACCESS1.3	22.1	66.1	-46.1	4.7	0.51	0.36	0.09	0.08	1.43	1.90	1.47	1.38
3	BCC-CSM1.1(m)	-21.0	-20.2	-30.9	-0.2	0.51	0.55	0.05	0.21	0.94	0.91	1.40	1.17
4	BCC-CSM1.1	25.4	17.2	36.0	34.0	0.29	0.03	0.08	0.03	1.43	1.23	2.28	1.92
5	BNU-ESM	23.6	70.8	-51.9	10.8	0.41	-0.15	0.12	0.17	1.40	1.82	1.40	1.55
6	CanESM2	-24.8	0.0	-53.6	-58.6	0.60	0.50	0.27	0.22	0.93	0.92	1.40	1.15
7	CCSM4	24.8	52.2	-53.8	102.6	0.41	0.19	-0.01	0.08	1.27	1.49	1.45	1.71
8	CESM1-BGC	22.4	54.9	-46.1	54.3	0.41	0.09	0.07	-0.01	1.28	1.54	1.58	1.41
9	CESM1-CAM5	44.7	78.2	-24.4	73.6	0.42	0.10	0.03	0.04	1.43	1.71	1.49	2.05
10	CMCC-CM	-49.9	-71.1	-40.9	17.2	0.17	0.30	0.12	0.25	1.20	1.50	1.29	1.43
11	CMCC-CMS	-16.7	-27.4	-31.0	62.8	0.40	0.56	0.02	0.22	1.00	0.94	1.36	1.64
12	CNRM-CM5	-33.2	-16.6	-55.2	-49.0	0.63	0.64	0.12	0.12	0.87	0.82	1.33	1.11
13	CSIRO-Mk3-6-0	-39.7	-63.5	-5.0	-25.2	0.18	0.41	0.02	-0.01	1.33	1.39	1.89	1.58
14	EC-EARTH	-11.6	0.8	-20.7	-41.5	0.48	0.33	0.14	-0.03	1.04	1.10	1.47	1.26
15	FGOALS-g2	83.1	137.9	6.9	40.1	0.59	0.47	0.15	0.17	1.78	2.54	1.44	1.53
16	GFDL-CM3	-16.0	-11.6	-59.9	73.2	0.39	0.43	0.06	0.20	1.12	1.03	1.40	2.05
17	GFDL-ESM2G	-27.2	-41.0	-45.4	75.1	0.08	-0.10	-0.10	0.14	1.25	1.26	1.65	1.92
18	GFDL-ESM2M	-26.1	-35.1	-51.1	72.6	0.06	-0.15	-0.07	0.04	1.33	1.39	1.67	2.07
19	HadGEM2-CC	12.5	41.3	-29.0	-6.7	0.56	0.57	0.08	0.10	1.06	1.08	1.49	1.38
20	HadGEM2-ES	8.6	43.6	-35.9	-28.9	0.57	0.62	-0.06	0.12	1.04	1.07	1.53	1.20
21	INMCM4.0	9.0	40.4	-66.0	61.4	0.45	0.34	-0.13	0.02	1.16	1.26	1.45	1.64
22	IPSL-CM5A-LR	-94.8	-94.4	-97.8	-89.1	0.23	0.17	0.09	0.14	1.41	1.83	1.61	1.20
23	IPSL-CM5A-MR	-73.3	-65.0	-91.1	-64.7	0.40	0.33	0.12	0.06	1.21	1.46	1.55	1.18
24	MIROC5	91.3	60.5	110.2	174.4	0.55	0.70	0.25	-0.05	1.68	1.54	2.30	2.78
25	MIROC5-ESM	82.8	117.0	8.1	122.3	0.48	0.25	0.04	0.25	1.80	2.32	1.64	2.40
26	MIROC5-ESM-CHEM	79.6	120.1	-1.2	107.7	0.48	0.28	0.04	0.14	1.78	2.35	1.64	2.15
27	MPI-ESM-LR	-32.8	-22.3	-47.8	-40.3	0.55	0.62	0.11	-0.03	0.94	0.86	1.38	1.33
28	MPI-ESM-MR	-7.0	6.0	-21.9	-24.5	0.55	0.61	0.12	0.05	0.95	0.81	1.50	1.31
29	MRI-CGCM3	-63.9	-85.6	-53.7	1.8	-0.08	-0.27	-0.02	0.17	1.41	1.79	1.48	1.65
30	NorESM1-M	16.2	32.3	-46.5	102.3	0.18	-0.43	0.08	0.07	1.47	1.70	1.54	2.28
31	MME	1.3	14.4	-31.7	27.2	0.60	0.64	0.13	0.20	0.82	0.83	1.15	1.13

Note: Blue font color – represents values for the best models, red font color – denotes values for the worst models and black font color – indicates values between the best and worst models.

with blue and red font colors. These tables were generated based on the MTS data between observed and historical GCM simulations.

The same analyses for T_{min}, at the annual temporal setting, proved that CMCC-CMS, MIROC5, CMCC-CM, BCC-CSM1.1, and GFDL-ESM2G based on PBIAS; the MME, CMCC-CM, CMCC-CMS, CNRM-CM5, and EC-EARTH in light of r [62,77,78]; and MIROC5, BCC-CSM1.1, BCC-CSM1.1 (m), BNU-ESM, and CMCC-CMS according to RSR, are the top-ranked five models with adequate proficiency in characterizing the observed T_{min} in the area. Likewise, the best-performing five GCMs with relatively strong capability in reproducing the observed T_{max} embrace CNRM-CM5, CanESM2, MRI-CGCM3, CMCC-CM, and CSIRO-Mk3-6-0 based on PBIAS [77]; the MME, CMCC-CMS, CMCC-CM, GFDL-CM3, and IPSL-CM5A-LR in light of r [62,78]; and CNRM-CM5, CanESM2, MRI-CGCM3, CMCC-CM, and CMCC-CMS, on the basis of RSR. A similar product, based on ATS data, which is not annexed to this manuscript, was also produced for the two variables to be considered in the MCDM analysis.

3.2. Ranking of GCMs with MCDM analysis

3.2.1. Approaches and procedures for ranking

The three SPMs (PBIAS, RSR, and r), in Table 5 below, particularly for the annual temporal scale, were considered for an example to establish the actual payoff matrix in Table 6 [Columns 2–5], and thus to demonstrate the MCDM approaches and procedures while ranking GCMs. A suitable data transformation was exercised in Table 6 [Columns 6–8] to lay the ideal groundwork for normalization with Eq. (4) and the construction of the normalized payoff matrix in Table 6 [Columns 9–11]. To determine the overall utility (U_a) for the WA method and L_p-metric values for the CP technique, the weights for each SPM were computed using the entropy method, as given in Eqs. (5)–(7). The entropy values (E_j) from the annual scale analysis were 0.92 for PBIAS, 0.99 for RSR, and 0.97 for r. Besides, the degree of diversification (D_j) for PBIAS, RSR, and r was 0.08, 0.01, and 0.03, respectively. Finally, the weights of the SPMs for the annual Pr were 0.68 (68%) for PBIAS, 0.06 (6%) for RSR, and 0.26 (26%) for r. The results have suggested that PBIAS is contributing the largest weight and has significant importance in the ranking process, followed by r, with the smallest contribution from RSR.

The U_a values for the GCMs were estimated using Eq. (8). Here, the negative values of PBIAS and RSR from the transformed payoff matrix (Table 6 [Columns 6 and 7]) and the actual calculated values of r (Table 6 [Column 5]) were considered in the WA method. Results for each model, including the MME, are provided in Table 6 [Column 12]. The alternatives (GCMs) with the highest overall utility were considered more suitable than others. Hence, the MME, MPI-ESM-MR, HadGEM2-ES, HadGEM2-CC, INMCM4.0, and EC-EARTH models took the top positions for Pr with the annual time scale (Table 6 [Column 13]).

Table 6
Ranking of GCMs with WA and CP methods for annual Pr over the MASB based on MTS data.

No.	GCMs	Calculated Performance Metric (Criteria) Values [Actual Payoff Matrix]			Transformed Payoff Matrix ($f_j(a)$)			Normalized Payoff Matrix with Method 3 ($V_j(a)/p_{ij}$)			Weighted Average (WA) Method		Transformed Payoff Matrix for Compromise Programming (CP)			Compromise Programming (CP) Method	
		PBIAS (%)	RSR (−)	r (−)	PBIAS	RSR	R	PBIAS	RSR	R	Overall Utility (U_a)	Rank	PBIAS	RSR	r	L_p-Metric (pA1)	Rank
[1]	[2]	[3]	[4]	[5]	[6]	[7]	[8]	[9]	[10]	[11]	[12]	[13]	[14]	[15]	[16]	[17]	[18]
1	ACCESS1.0	30.7	1.16	0.55	0.307	1.16	0.55	0.027	0.030	0.043	−0.133	14	−0.307	−1.158	0.548	0.263	14
2	ACCESS1.3	22.1	1.43	0.51	0.221	1.43	0.51	0.020	0.037	0.040	−0.100	11	−0.221	−1.432	0.509	0.231	11
3	BCC-CSM1.1(m)	−21.0	0.94	0.51	0.210	0.94	0.51	0.019	0.024	0.040	−0.064	7	−0.210	−0.935	0.510	0.193	8
4	BCC-CSM1.1	25.4	1.43	0.29	0.254	1.43	0.29	0.023	0.037	0.023	−0.181	19	−0.254	−1.433	0.290	0.336	19
5	BNU-ESM	23.6	1.40	0.41	0.236	1.40	0.41	0.021	0.036	0.032	−0.136	16	−0.236	−1.399	0.407	0.278	16
6	CanESM2	−24.8	0.93	0.60	0.248	0.93	0.60	0.022	0.024	0.047	−0.067	8	−0.248	−0.933	0.598	0.189	7
7	CCSM4	24.8	1.27	0.41	0.248	1.27	0.41	0.022	0.032	0.032	−0.136	17	−0.248	−1.265	0.406	0.279	17
8	CESM1-BGC	22.4	1.28	0.41	0.224	1.28	0.41	0.020	0.033	0.032	−0.120	13	−0.224	−1.284	0.412	0.261	13
9	CESM1-CAM5	44.7	1.43	0.42	0.447	1.43	0.42	0.040	0.037	0.033	−0.277	22	−0.447	−1.427	0.422	0.427	22
10	CMCC-CM	−49.9	1.20	0.17	0.499	1.20	0.17	0.045	0.031	0.013	−0.366	24	−0.499	−1.200	0.167	0.546	24
11	CMCC-CMS	−16.7	1.00	0.40	0.167	1.00	0.40	0.015	0.026	0.031	−0.068	9	−0.167	−1.004	0.401	0.207	9
12	CNRM-CM5	−33.2	0.87	0.63	0.332	0.87	0.63	0.030	0.022	0.049	−0.113	12	−0.332	−0.870	0.627	0.235	12
13	CSIRO-Mk3-6-0	−39.7	1.33	0.18	0.397	1.33	0.18	0.036	0.034	0.014	−0.301	23	−0.397	−1.328	0.178	0.475	23
14	EC-EARTH	−11.6	1.04	0.48	0.116	1.04	0.48	0.010	0.027	0.038	−0.014	6	−0.116	−1.041	0.481	0.142	5
15	FGOALS-g2	83.1	1.78	0.59	0.831	1.78	0.59	0.074	0.046	0.046	−0.516	26	−0.831	−1.783	0.587	0.667	26
16	GFDL-CM3	−16.0	1.12	0.39	0.160	1.12	0.39	0.014	0.029	0.030	−0.072	10	−0.160	−1.122	0.389	0.212	10
17	GFDL-ESM2G	−27.2	1.25	0.08	0.272	1.25	0.08	0.024	0.032	0.006	−0.237	20	−0.272	−1.255	0.080	0.416	20
18	GFDL-ESM2M	−26.1	1.33	0.06	0.261	1.33	0.06	0.023	0.034	0.005	−0.239	21	−0.261	−1.332	0.061	0.419	21
19	HadGEM2-CC	12.5	1.06	0.56	0.125	1.06	0.56	0.011	0.027	0.044	0.001	4	−0.125	−1.057	0.562	0.119	4
20	HadGEM2-ES	8.6	1.04	0.57	0.086	1.04	0.57	0.008	0.027	0.045	0.031	3	−0.086	−1.040	0.574	0.086	3
21	INMCM4.0	9.0	1.16	0.45	0.090	1.16	0.45	0.008	0.030	0.035	−0.012	5	−0.090	−1.157	0.448	0.142	6
22	IPSL-CM5A-LR	−94.8	1.41	0.23	0.948	1.41	0.23	0.085	0.036	0.018	−0.666	31	−0.948	−1.411	0.232	0.861	31
23	IPSL-CM5A-MR	−73.3	1.21	0.40	0.733	1.21	0.40	0.066	0.031	0.031	−0.465	25	−0.733	−1.212	0.398	0.632	25
24	MIROC5	91.3	1.68	0.55	0.913	1.68	0.55	0.082	0.043	0.043	−0.575	30	−0.913	−1.681	0.552	0.734	29
25	MIROC5-ESM	82.8	1.80	0.48	0.828	1.80	0.48	0.074	0.046	0.037	−0.544	29	−0.828	−1.803	0.477	0.707	28
26	MIROC5-ESM-CHEM	79.6	1.78	0.48	0.796	1.78	0.48	0.071	0.046	0.038	−0.519	27	−0.796	−1.785	0.482	0.680	27
27	MPI-ESM-LR	−32.8	0.94	0.55	0.328	0.94	0.55	0.029	0.024	0.043	−0.134	15	−0.328	−0.936	0.552	0.264	15
28	MPI-ESM-MR	−7.0	0.95	0.55	0.070	0.95	0.55	0.006	0.024	0.043	0.042	2	−0.070	−0.949	0.554	0.076	2
29	MRI-CGCM3	−63.9	1.41	−0.08	0.639	1.41	0.08	0.057	0.036	0.006	−0.539	28	−0.639	−1.411	−0.083	0.752	30
30	NorESM1-M	16.2	1.47	0.18	0.162	1.47	0.18	0.015	0.038	0.014	−0.149	18	−0.162	−1.467	0.180	0.311	18
31	MME	1.3	0.82	0.60	0.013	0.82	0.60	0.001	0.021	0.047	0.100	1	−0.013	−0.823	0.598	0.011	1
											Ideal values (f_j*)		−0.013	−0.823	0.627		

Similarly, the estimation of the L_p-metric for all GCMs involves the identification of ideal values (f_j*) and the estimation of weights for each SPM. The ideal values were −0.013 for PBIAS, −0.823 for RSR, and 0.627 for r, which is the maximum of Columns 14, 15, and 16 in Table 6 since the selected approach in this evaluation was a maximization perspective for uniform analysis. The SPM weights remain the same as computed above, and the p-value was chosen to be 1 while calculating the L_p-metric value using Eqs. 9 and 10. Like the WA approach, the computation of L_p-metrics would require negative values of PBIAS and RSR from the transformed payoff matrix and the actual calculated values of r in Table 6 [Columns 14, 15, and 16]. The GCMs with the smallest values of the L_p-metric were considered the best, as shown in Table 6 [Columns 17 and 18]. The analysis in Table 6 [Column 18] verified that the MME, MPI-ESM-MR, HadGEM2-ES, HadGEM2-CC, EC-EARTH, and INMCM4.0 are the top-ranked six GCMs for Pr with the same time scale adopting the CP method.

3.2.2. Ranking of GCMs based on MTS data

(a)Precipitation

The aggregation of ranks from the two methods and the overall aggregation of aggregated ranks for Pr, with the annual and seasonal temporal resolutions, followed the approach as outlined in Section 2.3.4 (E), and the findings are given in Table 7 below. For annual Pr, the top-ranked GCMs were the MME (1), MPI-ESM-MR (2), HadGEM2-ES (3), HadGEM2-CC (4), INMCM4.0 (5), and EC-EARTH (5), with the last two having similar ranks. Following the same analogy, aggregation of ranks for the seasonal Pr was achieved, and the ranks are provided in the same table. The best-performing GCMs that reproduced the major rainy season fairly in the MASB were MPI-ESM-MR (1), CanESM2 (2), MME (3), CNRM-CM5 (4), EC-EARTH (5), and MPI-ESM-LR (5). On the other hand, FGOALS-g2 (1), MIROC5-ESM-CHEM (2), ACCESS1.0 (3), EC-EARTH (3), MIROC5-ESM (5), and MPI-ESM-MR (5) were the most suitable GCMs, which were quite good at replicating the minor rainy season. Besides, BCC-CSM1.1(m) (1), CMCC-CM (2), MRI-CGCM3 (3), BNU-ESM (4), MME (5), ACCESS1.0 (6), ACCESS1.3 (6), and HadGEM2-CC (6), with the last three receiving equal ranks, were the top-positioned GCMs with sufficient capability to simulate the dry season rainfall in the sub-basin (Table 7).

(b) Minimum and maximum temperature

Considering the findings in Fig. 6 and Table C1 of the appendix, MIROC5 (1), BCC-CSM1.1 (2), BCC-CSM1.1(m) (3), CMCC-CMS (4), BNU-ESM (5), and MIROC5-ESM (6) are among the top-ranked six GCMs, which were quite good at duplicating the T_{min} adequately over the four temporal scales in the sub-basin. Moreover, the T_{max} for the annual and seasonal time scales was suitably replicated by the CNRM-CM5 (1), CMCC-CM (2), CanESM2 (3), CMCC-CMS (4), MRI-CGCM3 (5), and BCC-CSM1.1(m) (6) models, which show superior capability in simulating the variable of interest over the MASB. The BCC-CSM1.1(m) model, which stood 4th for Pr, 3rd for T_{min}, and 6th for T_{max}, was found competent in duplicating the 3 variables simultaneously under varying temporal settings

Table 7
Summary of ranks and aggregated ranks of GCMs for annual and seasonal Pr in the MASB based on MTS data.

No	GCMs	Temporal Resolutions, Ranks, Sum of Ranks and Aggregated Ranks																Sum of Agg. Ranks	Overall Aggregated Rank
		Annual				JJAS				FMAM				ONDJ					
		Rank [WA]	Rank [CP]	∑Ranks	Agg. Rank	Rank [WA]	Rank [CP]	∑Ranks	Agg. Rank	Rank [WA]	Rank [CP]	∑Ranks	Agg. Rank	Rank [WA]	Rank [CP]	∑Ranks	Agg. Rank		
1	ACCESS1.0	14	14	28	**14**	13	12	25	**12**	3	6	9	**3**	11	3	14	**6**	35	**7**
2	ACCESS1.3	11	11	22	**11**	22	21	43	**21**	17	17	34	**16**	4	10	14	**6**	54	**12**
3	BCC-CSM1.1(m)	7	8	15	**7**	7	7	14	**7**	11	14	25	**13**	1	1	2	**1**	28	**4**
4	BCC-CSM1.1	19	19	38	**19**	12	13	25	**12**	15	16	31	**15**	15	18	33	**16**	62	**16**
5	BNU-ESM	16	16	32	**16**	26	26	52	**26**	20	15	35	**18**	5	6	11	**4**	64	**17**
6	CanESM2	8	7	15	**7**	2	2	4	**2**	12	2	14	**7**	14	7	21	**11**	27	**3**
7	CCSM4	17	17	34	**17**	17	17	34	**17**	24	25	49	**24**	27	29	56	**29**	87	**25**
8	CESM1-BGC	13	13	26	**13**	21	22	43	**21**	19	21	40	**20**	19	26	45	**23**	77	**20**
9	CESM1-CAM5	22	22	44	**22**	25	25	50	**25**	10	12	22	**11**	26	27	53	**27**	85	**21**
10	CMCC-CM	24	24	48	**24**	23	23	46	**23**	13	11	24	**12**	3	2	5	**2**	61	**14**
11	CMCC-CMS	9	9	18	**9**	9	9	18	**9**	14	20	34	**16**	18	11	29	**14**	48	**9**
12	CNRM-CM5	12	12	24	**12**	4	4	8	**4**	22	18	40	**20**	13	13	26	**13**	49	**10**
13	CSIRO-Mk3-6-0	23	23	46	**23**	16	16	32	**16**	5	9	14	**7**	12	20	32	**15**	61	**14**
14	EC-EARTH	6	5	11	**5**	5	6	11	**5**	6	3	9	**3**	17	23	40	**20**	33	**6**
15	FGOALS-g2	26	26	52	**26**	31	31	62	**31**	1	1	2	**1**	10	9	19	**9**	67	**18**
16	GFDL-CM3	10	10	20	**10**	8	8	16	**8**	23	22	45	**22**	21	14	35	**17**	57	**13**
17	GFDL-ESM2G	20	20	40	**20**	19	20	39	**20**	26	29	55	**27**	23	16	39	**19**	86	**24**
18	GFDL-ESM2M	21	21	42	**21**	18	19	37	**18**	27	28	55	**27**	25	28	53	**27**	93	**28**
19	HadGEM2-CC	4	4	8	**4**	11	11	22	**11**	9	10	19	**10**	6	8	14	**6**	31	**5**
20	HadGEM2-ES	3	3	6	**3**	10	10	20	**10**	21	24	45	**22**	8	12	20	**10**	45	**8**
21	INMCM4.0	5	6	11	**5**	14	15	29	**14**	28	31	59	**30**	22	25	47	**24**	73	**19**
22	IPSL-CM5A-LR	31	31	62	**31**	27	27	54	**27**	30	30	60	**31**	24	17	41	**21**	110	**31**
23	IPSL-CM5A-MR	25	25	50	**25**	20	18	38	**19**	29	27	56	**29**	20	21	41	**21**	94	**29**
24	MIROC5	30	29	59	**30**	15	14	29	**14**	31	23	54	**26**	31	31	62	**31**	101	**30**
25	MIROC5-ESM	29	28	57	**28**	29	29	58	**29**	4	8	12	**5**	30	19	49	**25**	87	**25**
26	MIROC5-ESM-CHEM	27	27	54	**27**	30	30	60	**30**	2	4	6	**2**	28	24	52	**26**	85	**21**
27	MPI-ESM-LR	15	15	30	**15**	6	5	11	**5**	16	13	29	**14**	16	22	38	**18**	52	**11**
28	MPI-ESM-MR	2	2	4	**2**	1	1	2	**1**	7	5	12	**5**	9	15	24	**12**	20	**2**
29	MRI-CGCM3	28	30	58	**29**	28	28	56	**28**	25	26	51	**25**	2	4	6	**3**	85	**21**
30	NorESM1-M	18	18	36	**18**	24	24	48	**24**	18	19	37	**19**	29	30	59	**30**	91	**27**
31	MME	1	1	2	**1**	3	3	6	**3**	8	7	15	**9**	7	5	12	**5**	18	**1**

Note: Blue font color – represents overall aggregated ranks for best models and red font color – denotes ranks for worst models.

(Table C1 of the appendix). In addition, the results from a study made by Ref. [79] displayed BCC-CSM1.1(m) and CMCC-CMS as the best-performing GCMs for simulating T_{min} and T_{max} over Pakistan, which was partly consistent with the findings of this work.

3.2.3. Ranking of GCMs based on ATS data

(a) Precipitation

The top-ranked GCMs, based on ATS data, over the annual and seasonal temporal resolutions were identified in the MASB following the same approach as discussed above. Towards this end, six GCMs (MME (1), ACCESS1.0 (2), EC-EARTH (3), HadGEM2-CC (4), CanESM2 (5), and MPI-ESM-MR (6)) were quite good at representing annual Pr in the sub-basin (Table 8). Similar results were reported by Refs. [62,78] for the suitability of the MME compared to individual GCMs and RCMs. Moreover, the ability of EC-EARTH and CanESM2 to simulate Pr was also witnessed [79,80]. The capability of each model to duplicate the climate system of the sub-basin for each temporal scale is provided in the same table.

(b) Minimum and maximum temperature

The overall aggregated rank in Table 8 defines that BNU-ESM (1), MIROC5 (2), BCC-CSM1.1 (3), BCC-CSM1.1(m) (4), CMCC-CMS (5), and CMCC-CM (6) are the top-ranked models with superior potential in replicating the T_{min} over the four temporal scales. Likewise, six GCMs were identified as the most competent models for duplicating features of T_{max} over the annual and seasonal time scales. These are CMCC-CM (1), CanESM2 (2), IPSL-CM5A-LR (3), CNRM-CM5 (4), CMCC-CMS (5), and BCC-CSM1.1(m) (5), with the last two holding equal positions.

3.2.4. Aggregation of ranks from the MTS and ATS analysis

The aggregated ranks of the three variables resulting from the analyses, based on MTS and ATS data, over the four temporal scales displayed the best and worst GCMs for each variable, with the blue font colors for the best and the red ones for the worst models (Table 9). It can be seen from Table 9 that the MME (1), MPI-ESM-MR (2), CanESM2 (2), EC-EARTH (4), HadGEM2-CC (4), and ACCESS1.0 (4) are the top-ranked GCMs that have a satisfactory performance in characterizing the annual and seasonal Pr over the sub-basin [62,79,78,80]. Conversely, the least-performing GCMs encompass MIROC5-ESM (26), MIROC5-ESM-CHEM (26),

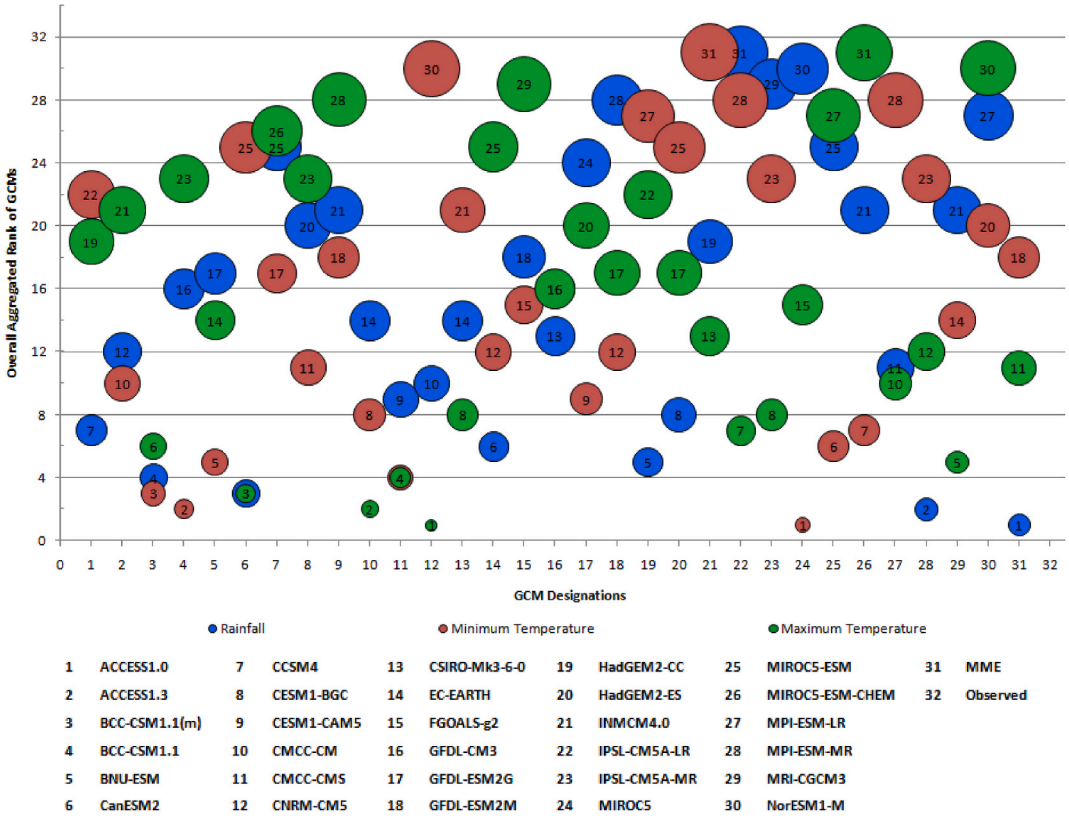

Fig. 6. Overall aggregated rank of GCMs for Pr, T_{min} and T_{max} based on MTS data in MSAB (small bubbles demonstrate best ranked GCMs with lowest sum of ranks and large bubbles for the opposite).

Table 8
Summary of aggregated ranks and overall aggregated ranks of GCMs for Pr, T_{min} and T_{max} over the four temporal scales in the MASB based on ATS data.

No	GCMs	Pr						T_{min}						T_{max}					
		Annual	JJAS	FMAM	ONDJ	∑Agg. Rank	Overall Agg. Rank	Annual	JJAS	FMAM	ONDJ	∑Agg. Rank	Overall Agg. Rank	Annual	JJAS	FMAM	ONDJ	∑Agg. Rank	Overall Agg. Rank
		Agg. Rank	Agg. Rank	Agg. Rank	Agg. Rank			Agg. Rank	Agg. Rank	Agg. Rank	Agg. Rank			Agg. Rank	Agg. Rank	Agg. Rank	Agg. Rank		
1	ACCESS1.0	2	16	3	5	26	**2**	25	14	19	23	81	**23**	7	17	2	7	33	**8**
2	ACCESS1.3	15	19	4	11	49	**7**	9	4	14	8	35	**7**	27	21	21	28	97	**27**
3	BCC-CSM1.1(m)	23	10	18	5	56	**15**	4	2	16	5	27	**4**	6	7	9	2	24	**5**
4	BCC-CSM1.1	16	6	7	24	53	**9**	2	20	1	3	26	**3**	21	26	8	10	65	**15**
5	BNU-ESM	19	26	1	9	55	**13**	6	3	3	11	23	**1**	11	20	2	17	50	**10**
6	CanESM2	6	3	5	19	33	**5**	27	5	28	29	89	**24**	4	9	1	1	15	**2**
7	CCSM4	9	10	9	26	54	**10**	12	6	16	11	45	**11**	26	23	14	17	80	**24**
8	CESM1-BGC	13	21	13	26	73	**21**	8	1	14	16	39	**9**	11	15	7	22	55	**11**
9	CESM1-CAM5	21	25	15	21	82	**23**	15	19	7	18	59	**15**	29	28	30	29	116	**30**
10	CMCC-CM	17	24	12	2	55	**13**	1	28	2	1	32	**6**	1	1	2	3	7	**1**
11	CMCC-CMS	12	8	24	10	54	**10**	2	18	4	4	28	**5**	3	5	6	10	24	**5**
12	CNRM-CM5	22	8	23	7	60	**17**	30	31	30	30	121	**31**	9	1	5	6	21	**4**
13	CSIRO-Mk3-6-0	13	17	20	13	63	**18**	21	12	25	15	73	**22**	13	5	25	19	62	**12**
14	EC-EARTH	2	1	14	11	28	**3**	11	12	7	14	44	**10**	19	24	27	8	78	**22**
15	FGOALS-g2	24	30	1	14	69	**20**	19	30	12	10	71	**20**	21	29	21	14	85	**25**
16	GFDL-CM3	8	5	22	14	49	**7**	12	7	10	22	51	**13**	16	11	12	24	63	**13**
17	GFDL-ESM2G	18	20	25	23	86	**25**	14	22	16	6	58	**14**	18	17	24	20	79	**23**
18	GFDL-ESM2M	24	23	19	28	94	**28**	9	23	6	7	45	**11**	25	16	29	26	96	**26**
19	HadGEM2-CC	7	13	7	3	30	**4**	29	25	29	27	110	**29**	19	22	19	9	69	**18**
20	HadGEM2-ES	2	13	26	16	57	**16**	28	23	20	28	99	**27**	15	24	16	12	67	**16**
21	INMCM4.0	5	12	29	22	68	**19**	30	25	31	31	117	**30**	10	14	20	23	67	**16**
22	IPSL-CM5A-LR	31	26	31	25	113	**31**	23	16	26	25	90	**25**	2	3	9	4	18	**3**
23	IPSL-CM5A-MR	27	21	29	16	93	**27**	17	10	22	19	68	**18**	17	7	26	20	70	**19**
24	MIROC5	29	13	26	31	99	**29**	6	8	9	2	25	**2**	24	9	13	24	70	**19**
25	MIROC5-ESM	30	28	11	18	87	**26**	15	20	12	13	60	**16**	28	26	28	30	112	**29**
26	MIROC5-ESM-CHEM	26	30	20	28	104	**30**	19	27	4	17	67	**17**	30	29	31	31	121	**31**
27	MPI-ESM-LR	11	7	16	20	54	**10**	23	16	26	25	90	**25**	7	12	11	12	42	**9**
28	MPI-ESM-MR	10	3	16	8	37	**6**	17	10	22	19	68	**18**	14	13	21	15	63	**13**
29	MRI-CGCM3	27	28	26	1	82	**23**	5	14	10	9	38	**8**	4	3	16	5	28	**7**
30	NorESM1-M	20	17	6	30	73	**21**	26	28	24	24	102	**28**	30	31	16	26	103	**28**
31	MME	1	2	10	4	17	**1**	22	9	21	19	71	**20**	23	19	15	16	73	**21**

Note: Blue font color – represents overall aggregated ranks for best models and red font color – denotes ranks for worst models.

IPSL-CM5A-MR (28), GFDL-ESM2M (28), MIROC5 (30), and IPSL-CM5A-LR (31) which reveals very weak skill in duplicating the Pr in the MASB.

Similarly, the best models that show improved potential in replicating the annual and seasonal T_{min} over the MASB include MIROC5 (1), BCC-CSM1.1 (2), BNU-ESM (3), BCC-CSM1.1(m) (4), CMCC-CMS (5), and CMCC-CM (6) [79,81]. Conversely, HadGEM2-ES (26), IPSL-CM5A-LR (27), MPI-ESM-LR (27), HadGEM2-CC (29), CNRM-CM5 (30), and INMCM4.0 (30) were the least

Table 9
Summary of ranks of GCMs for Pr, T_{min} and T_{max} based on MTS and ATS data formats over the MASB.

No	GCMs	Climate Variables and Ranks												Aggregated Rank for the 3 Variables	
		(Pr				T_{min}				T_{max}					
		Ranks from MTS	Ranks from ATS	∑Rank	Final Rank	Ranks from MTS	Ranks from ATS	∑Rank	Final Rank	Ranks from MTS	Ranks from ATS	∑Rank	Final Rank	∑Rank	Last Rank
1	ACCESS1.0	7	2	9	**4**	22	23	45	**23**	19	8	27	**12**	39	**11**
2	ACCESS1.3	12	7	19	**7**	10	7	17	**7**	21	27	48	**25**	39	**11**
3	BCC-CSM1.1(m)	4	15	19	**7**	3	4	7	**4**	6	5	11	**6**	17	**2**
4	BCC-CSM1.1	16	9	25	**13**	2	3	5	**2**	23	15	38	**20**	35	**7**
5	BNU-ESM	17	13	30	**16**	5	1	6	**3**	14	10	24	**10**	29	**4**
6	CanESM2	3	5	8	**2**	25	24	49	**25**	3	2	5	**2**	29	**4**
7	CCSM4	25	10	35	**18**	17	11	28	**15**	26	24	50	**26**	59	**21**
8	CESM1-BGC	20	21	41	**21**	11	9	20	**8**	23	11	34	**18**	47	**16**
9	CESM1-CAM5	21	23	44	**22**	18	15	33	**17**	28	30	58	**29**	68	**29**
10	CMCC-CM	14	13	27	**14**	8	6	14	**6**	2	1	3	**1**	21	**3**
11	CMCC-CMS	9	10	19	**7**	4	5	9	**5**	4	5	9	**4**	16	**1**
12	CNRM-CM5	10	17	27	**14**	30	31	61	**30**	1	4	5	**2**	46	**14**
13	CSIRO-Mk3-6-0	14	18	32	**17**	21	22	43	**22**	8	12	20	**9**	48	**17**
14	EC-EARTH	6	3	9	**4**	12	10	22	**9**	25	22	47	**24**	37	**9**
15	FGOALS-g2	18	20	38	**19**	15	20	35	**18**	29	25	54	**27**	64	**28**
16	GFDL-CM3	13	7	20	**10**	16	13	29	**16**	16	13	29	**14**	40	**13**
17	GFDL-ESM2G	24	25	49	**25**	9	14	23	**12**	20	23	43	**22**	59	**21**
18	GFDL-ESM2M	28	28	56	**28**	12	11	23	**12**	17	26	43	**22**	62	**24**
19	HadGEM2-CC	5	4	9	**4**	27	29	56	**29**	22	18	40	**21**	54	**19**
20	HadGEM2-ES	8	16	24	**12**	25	27	52	**26**	17	16	33	**17**	55	**20**
21	INMCM4.0	19	19	38	**19**	31	30	61	**30**	13	16	29	**14**	63	**25**
22	IPSL-CM5A-LR	31	31	62	**31**	28	25	53	**27**	7	3	10	**5**	63	**25**
23	IPSL-CM5A-MR	29	27	56	**28**	23	18	41	**20**	8	19	27	**12**	60	**23**
24	MIROC5	30	29	59	**30**	1	2	3	**1**	15	19	34	**18**	49	**18**
25	MIROC5-ESM	25	26	51	**26**	6	16	22	**9**	27	29	56	**28**	63	**25**
26	MIROC5-ESM-CHEM	21	30	51	**26**	7	17	24	**14**	31	31	62	**31**	71	**30**
27	MPI-ESM-LR	11	10	21	**11**	28	25	53	**27**	10	9	19	**8**	46	**14**
28	MPI-ESM-MR	2	6	8	**2**	23	18	41	**20**	12	13	25	**11**	33	**6**
29	MRI-CGCM3	21	23	44	**22**	14	8	22	**9**	5	7	12	**7**	38	**10**
30	NorESM1-M	27	21	48	**24**	20	28	48	**24**	30	28	58	**29**	77	**31**
31	MME	1	1	2	**1**	18	20	38	**19**	11	21	32	**16**	36	**8**

Note: Blue font color – represents final ranks for best models and red font color – denotes ranks for worst models.

performing GCMs with the worst efficiency in representing T_{min} in the area. Correspondingly, GCMs with a good ability to mimic the characters of annual and seasonal T_{max} comprise CMCC-CM (1), CanESM2 (2), CNRM-CM5 (2), CMCC-CMS (4), IPSL-CM5A-LR (5), and BCC-CSM1.1(m) (6) [79,81]. In contrast, the poorly performing GCMs with unsatisfactory performance for T_{max} were CCSM4 (26), FGOALS-g2 (27), MIROC5-ESM (28), CESM1-CAM5 (29), NorESM1-M (29), and MIROC5-ESM-CHEM (31) (Table 9).

In summary, the GCMs with adequate capability in simulating the characteristics of Pr, T_{min}, and T_{max} concurrently at the four temporal resolutions, based on MTS and ATS data, over the sub-basin were CMCC-CMS (1), BCC-CSM1.1(m) (2), CMCC-CM (3), BNU-ESM (4), CanESM2 (4), and MPI-ESM-MR (6) [79,82,81]. However, INMCM4.0 (25), IPSL-CM5A-LR (25), MIROC5-ESM (25), FGOALS-g2 (28), CESM1-CAM5 (29), MIROC5-ESM-CHEM (30), and NorESM1-M (31) were the least performing models to reproduce the features of the three variables at a time.

4. Discussion

The findings in Table 4 have confirmed that models that were best for one climate variable at a specific time scale may not always fit for other temporal resolutions [79]. Likewise, the most suitable models at one temporal scale for different climatic variables may not perform well at other temporal resolutions and data formats (MTS and ATS). It is obvious from the same table that the MME was not among the worst GCMs over a set of temporal scales, which attests to the value addition achieved through ensembling a subset of models rather than the application of individual GCMs. Besides, most of the GCMs, among the best and worst models, were characterized by an overestimation of the mean observed Pr (Table 4).

Many GCMs in the annual temporal setting overestimated the observed Pr variability except for a few models, including the MME, which were in the low variability class (Fig. 4). Yet, the variability of observed Pr in the major rainy season was underestimated by multiple GCMs. Conversely, the variability in the minor rainy season was overestimated by several models, excluding six GCMs and the MME. Similar to the Pr variability in the JJAS season, most GCMs, with the exception of four, underestimated the variability during the dry season, as given in Fig. 4 above.

The performance evaluation of GCMs for precipitation, on the basis of the correlation coefficient, confirms that the magnitude of linear association was much stronger in the JJAS season as compared to the others and became very weak for the FMAM and ONDJ seasons (Table 5).

The research conducted by Ref. [77] in Ziway Lake basin with 3 CMIP5 GCMs (CNRM-CM5, MPI-ESM-LR, and CSIRO-Mk3-6-0) demonstrated the reasonable suitability of these models, based on PBIAS, RMSE, and r, in simulating both monthly precipitation and temperature, which is much more consistent with the findings resulting from the performance evaluation of GCMs using PBIAS, RSR, and r in this study over a range of temporal scales. Also, the superiority of the MME was justified by a study made by Ref. [78] at simulating precipitation in the Upper Awash sub-basin using four performance metrics: PBIAS, CV, RMSE, and r, and the same was also realized in this study at various temporal resolutions.

In general, it can be concluded that different models respond differently to the various performance metrics over a range of temporal resolutions and data formats. Thus, it looks very difficult to find a common model that works best for all climate variables under various conditions. In this connection, the need for proper ranking and selection of models with a viable approach and performance metrics for various climate variables over multiple situations is mandatory to develop a subset of best-performing GCMs that can reproduce the observed climate system over a certain area of interest.

In a nutshell, the overall aggregated rank for Pr, based on MTS data, over the four temporal resolutions illustrated that the MME (1), MPI-ESM-MR (2), CanESM2 (3), BCC-CSM1.1(m) (4), HadGEM2-CC (5), and EC-EARTH (6) were the top-ranked six models with superior skill in characterizing the Pr in the sub-basin (Table 7 and Fig. 6). The findings from similar studies [62,78] revealed the superior advantage of the MME over many other individual models. Also, the EC-EARTH model received the first position among 36 GCMs for a study conducted in Pakistan using six spatial metrics [79]. Another two evaluations have confirmed the capability of CanESM2 [80] and BCC-CSM1.1 [83] in simulating precipitation adequately in India.

The selected models were comparatively better at reproducing the Pr during the annual and seasonal time settings. The findings in this study prove that a model that works fine for a specific temporal scale will not always produce the same results for another time setting. Hence, proper evaluation of the GCMs' skill at each time scale and aggregating the ranks achieved from each analysis are very crucial to establishing the ensemble of best GCMs that capture the real climate system of the area for the chosen variable under a certain time scale and data format. The attempt made by Ref. [82] to evaluate 21 GCMs in the Awash basin based on four metrics confirmed that MPI-ESM-MR, MPI-ESM-LR, GFDL-CM3, and HadGEM2-AO are the best-performing GCMs, which were somewhat consistent with the findings of this study.

According to the analysis made with the MTS data, the MMEs of the 30 GCMs, which were supposed to be superior to the individual models, were not among the top-ranked six models, both for T_{min} and T_{max}. However, it attains the 18th and 11th ranks for T_{min} and T_{max}, respectively, which still verifies its comparative skill over the worst or least suitable GCMs (Fig. 6 and Table C1 of the appendix). The MME will produce an acceptable result provided that the GCMs in the subset of models for ensembling are carefully selected. The shortlisted models should also be sufficiently capable of representing the characteristics of the climatic variables over a range of spatial and temporal scales under varying circumstances. Therefore, the best GCMs from the long list of models should be used while establishing time series data for the MME with suitable ensembling techniques.

The ranking of GCMs on the basis of ATS data demonstrated that the MME was among the top-ten GCMs over a range of seasons, which signifies its superior potential in mimicking the Pr characteristics under varying time scales. However, the most suitable models from one temporal setting were unable to simultaneously simulate the Pr features across the other temporal resolutions (Table 8). The findings for T_{min} and T_{max} in this study (Table 8) were reinforced by Ref. [79] and suggested two GCMs (BCC-CSM1.1(m) and CMCC-CMS) as the best-performing models in duplicating both T_{min} and T_{max} over Pakistan. In addition, three models, i.e., BCC-CSM1.1(m), CMCC-CM, and CMCC-CMS, satisfactorily and consistently simulated both the T_{min} and T_{max} simultaneously over the MASB.

The aggregation of ranks from the MTS and ATS analyses in Table 9 asserts the superior skill and performance of the MME in representing the climate of the study area compared to many other individual GCMs. The overall findings from this work have illustrated that, instead of aggregating the ranks from the three variables into one, it is rather wise to treat each variable independently to establish a subset of the best GCMs for MME since each GCM responds significantly differently to each variable under a set of conditions.

Finally, evaluating the skills of GCMs in duplicating the observed Pr, T_{min}, and T_{max} is essential for projecting future climate and further investigating climate change impact assessment and hydrological modeling in the study area. Besides, the approaches in this study can be extrapolated to other GCMs and RCMs, climate variables, and regions with multiple performance metrics, different MCDM techniques for ranking, and the suitable selection of a subset of skilled GCMs for ensembling to minimize uncertainties in the GCM projections. Towards this end, the recently released CMIP6 datasets will provide a greater opportunity to further examine, compare, rank, and select the most suitable models between the CMIP5 and CMIP6 GCMs in the study area and beyond.

5. Conclusion

This study concentrates on the performance evaluation of 30 CMIP5 GCMs, including the MME, in reproducing the observed Pr, T_{min}, and T_{max} over the MASB. The 1981–2005 baseline periods were considered for the analyses using MTS and ATS data formats over the annual and seasonal temporal scales. Essentially, two approaches were followed to measure the skill of GCMs. The first one was an evaluation of the GCMs with 5 SPMs (mean, CV, PBIAS, RSR, and r) taking observed and raw historical GCM simulations as input data. Meanwhile, the second approach involves the use of MCDM analysis using three SPMs (PBIAS, RSR, and r) to determine the relative performance of models in replicating the observed climate. Besides, the weights of the SPMs were managed through the entropy method. Also, two MCDM techniques, i.e., WA and CP, were employed for the ranking and selection of the best GCMs at a sub-basin scale. The main findings of this study are summarized below.

The evaluation of GCMs using 5-SPMs illustrates that a GCM that performs well for one SPM for a specific variable may fail to achieve the same for another SPM on the same temporal scale. Likewise, for the same SPM at different resolutions, a GCM may perform well on one time scale but poorly on another. These suggested that the outputs of GCM skills for a particular variable of interest relied mainly on the performance metrics, data format, and time scale chosen for analyses. Thus, it is very critical to evaluate the performance of GCMs using multiple performance metrics over a range of spatial and temporal settings and data formats for various climate variables rather than a single consideration alone.

Outcomes of the MCDM analysis confirmed that the MME, MPI-ESM-MR, CanESM2, EC-EARTH, HadGEM2-CC, and ACCESS1.0 were the most skillful GCMs in simulating the time series characteristics of Pr over the four temporal settings in the sub-basin. Similarly, MIROC5, BCC-CSM1.1, BNU-ESM, BCC-CSM1.1(m), CMCC-CMS, and CMCC-CM occupied the top positions in replicating the annual and seasonal T_{min}. Also, the best-performing GCMs in duplicating the features of T_{max} encompass CMCC-CM, CanESM2, CNRM-CM5, CMCC-CMS, IPSL-CM5A-LR, and BCC-CSM1.1(m). However, it was noticed that different GCMs performed much differently in duplicating various variables over a set of temporal scales and data formats.

In brief, the ensemble of GCMs that asserts adequate performance in simulating the salient features of Pr, T_{min}, and T_{max} concomitantly over the MASB includes CMCC-CMS (1), BCC-CSM1.1(m) (2), CMCC-CM (3), BNU-ESM (4), CanESM2 (4), and MPI-ESM-MR (6). Conversely, INMCM4.0 (25), IPSL-CM5A-LR (25), MIROC5-ESM (25), FGOALS-g2 (28), CESM1-CAM5 (29), MIROC5-ESM-CHEM (30), and NorESM1-M (31) were incapable of reproducing the statistical characteristics of the three climate variables at a time. Amazingly, none of the best models were able to consistently simulate the three variables at a time over a range of data formats and temporal resolutions.

In addition, the MME, which holds the 8th rank in the overall aggregated matrix, proves its superior potential in representing the climate of the study area compared to many other individual GCMs. The overall findings from this work indicated that, instead of aggregating the ranks of the three variables into one, it is good to treat each variable independently while developing a subset of best-performing GCMs for ensembling since each GCM responds much differently to each variable under a range of considerations.

The performance evaluation of GCMs with a diverse set of performance metrics, temporal resolutions, data formats, and several MCDM methods is crucial to determining the relative performance of models in replicating the observed climate under a subset of conditions. This, in turn, helps with the ranking and selection of the most suitable models for subsequent endeavors. However, given the limitations in resources, time, and scope of the work, this study mainly concentrates on evaluating the skills of 30 CMIP5 GCMs with only three SPMs (PBIAS, RSR, and r), at reproducing three climate variables (Pr, T_{min}, and T_{max}) using only two MCDM techniques (WA and CP).

Author contribution statement

Endalkachew Tesfaye: Conceived and designed the experiments; Performed the experiments; Analyzed and interpreted the data; Contributed reagents, materials, analysis tools or data; Wrote the paper.

Brook Abate; Taye Alemayehu and Yihun Dile: Analyzed and interpreted the data; Contributed reagents, materials, analysis tools or data; Wrote the paper.

Data availability statement

The authors do not have permission to share data.

Declaration of competing interest

The authors declare that they have no known competing financial interests or personal relationships that could have appeared to influence the work reported in this paper.

Acknowledgements

The researchers are grateful to the Global Earth System Grid Federation for supplying the CMIP5 historical GCM simulations through the Global ESGF web portal (https://esgf-index1.ceda.ac.uk). We would also like to thank the National Meteorological Agency (NMA) of Ethiopia for its support in providing both the observed station and gridded data sets for the three variables at a daily time scale over the baseline period and spatial domain.

Appendix A

Table A1
Mean monthly Pr, T_{min} and T_{max} of GCMs, MME and observed data over the MASB based on MTS data (1981–2005)

No	GCMs	Mean Monthly Pr (mm)				Mean Monthly T_{min} (°C)				Mean Monthly T_{max} (°C)			
		Annual	JJAS	FMAM	ONDJ	Annual	JJAS	FMAM	ONDJ	Annual	JJAS	FMAM	ONDJ
1	ACCESS1.0	75.7	140.0	52.1	34.9	14.3	17.3	13.9	11.7	27.2	26.8	29.2	25.4
2	ACCESS1.3	70.7	158.3	30.0	21.8	15.2	18.2	14.7	12.7	25.8	26.7	27.5	23.3
3	BCC-CSM1.1(m)	45.7	76.1	38.5	22.7	16.2	19.0	15.7	14.0	29.2	31.6	29.8	26.1
4	BCC-CSM1.1	72.6	111.7	75.7	30.5	16.6	16.9	17.5	15.3	26.9	25.5	28.7	26.5
5	BNU-ESM	71.6	162.8	26.8	25.2	15.9	18.0	16.2	13.5	27.3	26.7	29.8	25.5
6	CanESM2	43.5	93.4	25.8	9.4	12.2	17.5	11.7	7.4	32.2	31.1	34.2	31.3
7	CCSM4	72.3	145.1	25.8	46.1	14.9	17.9	14.3	12.5	25.4	26.1	28.0	22.2
8	CESM1-BGC	70.9	147.6	30.0	35.1	15.1	18.0	14.6	12.6	25.8	26.2	28.4	22.7
9	CESM1-CAM5	83.8	169.9	42.1	39.5	14.9	17.7	14.8	12.4	24.9	24.1	27.7	23.0
10	CMCC-CM	29.0	27.5	32.9	26.7	18.1	21.7	17.7	14.8	30.0	33.3	30.0	26.6
11	CMCC-CMS	48.2	69.2	38.4	37.0	17.5	20.9	17.0	14.6	29.2	31.7	29.7	26.3
12	CNRM-CM5	38.7	79.5	24.9	11.6	10.4	14.0	10.2	7.0	33.2	34.1	35.3	30.1
13	CSIRO-Mk3-6-0	34.9	34.8	52.9	17.0	14.8	19.0	13.7	11.8	29.3	32.9	29.1	26.0
14	EC-EARTH	51.2	96.1	44.2	13.3	15.0	17.6	15.1	12.3	25.8	26.0	26.9	24.6
15	FGOALS-g2	106.0	226.7	59.6	31.8	14.7	15.1	15.9	13.1	24.4	22.5	26.7	23.9
16	GFDL-CM3	48.6	84.2	22.3	39.4	15.6	19.4	16.1	11.4	27.7	29.4	29.7	23.9
17	GFDL-ESM2G	42.2	56.3	30.4	39.8	18.4	20.8	18.9	15.4	27.0	28.2	29.1	23.6
18	GFDL-ESM2M	42.8	61.9	27.2	39.2	18.8	21.2	19.3	15.8	27.4	28.7	29.4	24.0
19	HadGEM2-CC	65.2	134.7	39.6	21.2	12.3	15.7	11.7	9.6	26.9	26.2	29.2	25.1
20	HadGEM2-ES	62.9	136.8	35.7	16.2	12.7	16.2	12.2	9.9	27.1	26.4	29.5	25.5
21	INMCM4.0	63.1	133.8	18.9	36.7	7.7	15.9	3.7	3.4	27.5	28.1	30.0	24.4
22	IPSL-CM5A-LR	3.0	5.3	1.2	2.5	11.3	15.9	9.8	8.2	28.8	32.1	29.1	25.2
23	IPSL-CM5A-MR	15.4	33.4	4.9	8.0	13.1	16.2	12.7	10.5	28.5	30.9	29.0	25.6
24	MIROC5	110.8	153.0	117.1	62.4	17.1	19.1	17.2	15.0	27.4	28.8	27.7	25.8
25	MIROC5-ESM	105.9	206.8	60.2	50.6	15.3	16.6	16.3	13.1	24.1	23.4	27.4	21.3
26	MIROC5-ESM-CHEM	104.0	209.8	55.1	47.2	15.4	16.7	16.3	13.2	24.2	23.4	27.6	21.4
27	MPI-ESM-LR	38.9	74.0	29.1	13.6	11.3	15.9	9.8	8.2	28.5	30.4	29.4	25.7
28	MPI-ESM-MR	53.9	101.0	43.5	17.2	13.1	16.2	12.7	10.5	27.9	29.5	28.8	25.5
29	MRI-CGCM3	20.9	13.7	25.8	23.1	16.2	19.9	15.8	12.9	30.8	34.7	31.1	26.6
30	NorESM1-M	67.3	126.1	29.8	46.0	14.5	16.2	14.9	12.4	23.8	22.7	26.7	21.9
31	MME	68.7	109.1	38.0	28.9	14.6	17.7	14.4	11.8	27.5	28.3	29.2	25.0
32	**Observed**	**57.9**	**95.3**	**55.7**	**22.7**	**17.4**	**18.8**	**17.7**	**15.8**	**33.5**	**34.7**	**34.4**	**31.4**

Note: Values typed with red and blue font colors demonstrate overestimation and underestimation of the observed mean values correspondingly. However, the best (minimum departures from the observed mean values) and the worst (considerable departures from the observed mean values) five GCMs from each were shaded with bright green and yellow colors respectively for quick identification in the table.

Table A2
Rank of best and worst GCMs for Pr, T_{min} and T_{max} over the annual and seasonal temporal scales based on MTS data

Annual (Jan-Dec) Temporal Scale												
No.	Mean Pr				Mean T_{min}				Mean T_{max}			
	Best GCMs	Rank	Worst GCMs	Rank	Best GCMs	Rank	Worst GCMs	Rank	Best GCMs	Rank	Worst GCMs	Rank
1	MME	1	MIROC5-ESM-CHEM	27	CMCC-CMS	1	CanESM2	27	CNRM-CM5	1	CESM1-CAM5	27
2	MPI-ESM-MR	2	MIROC5-ESM	28	MIROC5	2	IPSL-CM5A-LR	28	CanESM2	2	FGOALS-g2	28
3	HadGEM2-ES	3	FGOALS-g2	29	CMCC-CM	3	MPI-ESM-LR	28	MRI-CGCM3	3	MIROC5-ESM-CHEM	29
4	INMCM4.0	4	MIROC5	30	BCC-CSM1.1	4	CNRM-CM5	30	CMCC-CM	4	MIROC5-ESM	30
5	EC-EARTH	5	IPSL-CM5A-LR	31	GFDL-ESM2G	5	INMCM4.0	31	CSIRO-Mk3-6-0	5	NorESM1-M	31
JJAS Temporal Scale (Major Rainy Season)												
No.	Mean Pr				Mean T_{min}				Mean T_{max}			
	Best GCMs	Rank	Worst GCMs	Rank	Best GCMs	Rank	Worst GCMs	Rank	Best GCMs	Rank	Worst GCMs	Rank
1	CanESM2	1	MRI-CGCM3	27	BCC-CSM1.1(m)	1	IPSL-CM5A-LR	27	MRI-CGCM3	1	CESM1-CAM5	27
2	EC-EARTH	2	IPSL-CM5A-LR	28	CSIRO-Mk3-6-0	1	MPI-ESM-LR	27	CNRM-CM5	2	MIROC5-ESM	28
3	MPI-ESM-MR	3	MIROC5-ESM	29	MIROC5	3	HadGEM2-CC	29	CMCC-CM	3	MIROC5-ESM-CHEM	28
4	GFDL-CM3	4	MIROC5-ESM-CHEM	30	ACCESS1.3	4	FGOALS-g2	30	CSIRO-Mk3-6-0	4	NorESM1-M	30
5	MME	5	FGOALS-g2	31	GFDL-CM3	4	CNRM-CM5	31	IPSL-CM5A-LR	5	FGOALS-g2	31
FMAM Temporal Scale (Minor Rainy Season)												
No.	Mean Pr				Mean T_{min}				Mean T_{max}			
	Best GCMs	Rank	Worst GCMs	Rank	Best GCMs	Rank	Worst GCMs	Rank	Best GCMs	Rank	Worst GCMs	Rank
1	MIROC5-ESM-CHEM	1	GFDL-CM3	27	CMCC-CM	1	HadGEM2-CC	27	CanESM2	1	ACCESS1.3	27
2	CSIRO-Mk3-6-0	2	INMCM4.0	28	BCC-CSM1.1	2	CNRM-CM5	28	CNRM-CM5	2	MIROC5-ESM	27
3	ACCESS1.0	3	IPSL-CM5A-MR	29	MIROC5	3	IPSL-CM5A-LR	29	MRI-CGCM3	3	EC-EARTH	29
4	FGOALS-g2	4	IPSL-CM5A-LR	30	CMCC-CMS	4	MPI-ESM-LR	29	CMCC-CM	4	FGOALS-g2	30
5	MIROC5-ESM	5	MIROC5	31	GFDL-ESM2G	5	INMCM4.0	31	INMCM4.0	4	NorESM1-M	31
ONDJ Temporal Scale (Dry Season)												
No.	Mean Pr				Mean T_{min}				Mean T_{max}			
	Best GCMs	Rank	Worst GCMs	Rank	Best GCMs	Rank	Worst GCMs	Rank	Best GCMs	Rank	Worst GCMs	Rank
1	BCC-CSM1.1(m)	1	NorESM1-M	27	GFDL-ESM2M	1	IPSL-CM5A-LR	27	CanESM2	1	CESM1-BGC	27
2	MRI-CGCM3	2	CCSM4	28	GFDL-ESM2G	2	MPI-ESM-LR	27	CNRM-CM5	2	CCSM4	28
3	ACCESS1.3	3	MIROC5-ESM-CHEM	29	BCC-CSM1.1	3	CanESM2	29	CMCC-CM	3	NorESM1-M	29
4	HadGEM2-CC	4	MIROC5-ESM	30	MIROC5	4	CNRM-CM5	30	MRI-CGCM3	3	MIROC5-ESM-CHEM	30
5	BNU-ESM	5	MIROC5	31	CMCC-CM	5	INMCM4.0	31	BCC-CSM1.1	5	MIROC5-ESM	31

Note: GCMs typed with red font colors represent overestimation and the blue font colors demonstrate underestimation of mean values by the GCMs against the observed data.

Appendix B

Table B1
PBIAS, r and RSR between observed and historical GCM simulations for annual and seasonal T_{min} over the MASB based on MTS data (1981–2005)

No	GCMs	PBIAS				R				RSR			
		Annual	JJAS	FMAM	ONDJ	Annual	JJAS	FMAM	ONDJ	Annual	JJAS	FMAM	ONDJ
1	ACCESS1.0	-17.8	-8.1	-21.2	-25.6	0.73	-0.27	0.50	0.47	2.25	2.81	3.45	3.60
2	ACCESS1.3	-12.8	-3.1	-17.1	-19.4	0.79	0.02	0.67	0.54	1.73	1.57	2.81	2.75
3	BCC-CSM1.1(m)	-6.9	0.8	-11.2	-11.4	0.78	0.33	0.62	0.56	1.30	1.31	2.13	2.02
4	BCC-CSM1.1	-5.0	-10.2	-1.1	-3.3	0.62	0.31	0.61	0.48	1.01	2.89	1.01	1.28
5	BNU-ESM	-8.9	-4.5	-8.6	-14.5	0.77	0.33	0.61	0.34	1.33	1.55	1.89	2.29
6	CanESM2	-30.0	-6.9	-34.1	-53.1	0.79	-0.14	0.57	0.60	3.96	2.55	5.47	7.29
7	CCSM4	-14.4	-4.8	-18.9	-21.0	0.76	0.17	0.65	0.48	2.01	1.73	3.35	3.12
8	CESM1-BGC	-13.5	-4.2	-17.2	-20.4	0.76	0.36	0.62	0.47	1.90	1.51	3.13	3.01
9	CESM1-CAM5	-14.3	-6.2	-16.5	-21.7	0.75	-0.19	0.66	0.45	2.00	2.09	2.98	3.37
10	CMCC-CM	3.6	15.0	0.3	-6.3	0.82	0.09	0.67	0.62	1.48	4.16	1.56	1.87
11	CMCC-CMS	0.4	11.0	-3.7	-7.7	0.80	0.36	0.62	0.60	1.42	3.15	1.92	1.95
12	CNRM-CM5	-40.3	-25.4	-42.2	-56.0	0.80	0.01	0.62	0.52	4.46	6.87	6.24	7.29
13	CSIRO-Mk3-6-0	-15.0	1.1	-22.7	-25.6	0.75	-0.39	0.65	0.58	2.46	1.61	4.05	3.95
14	EC-EARTH	-13.9	-6.4	-14.5	-22.1	0.80	0.32	0.65	0.56	1.85	2.49	2.54	3.18
15	FGOALS-g2	-15.8	-19.7	-10.3	-17.2	0.66	0.43	0.55	0.52	1.86	5.25	1.86	2.43
16	GFDL-CM3	-10.4	3.0	-8.9	-27.9	0.78	0.21	0.59	0.47	2.22	2.40	2.82	4.09
17	GFDL-ESM2G	5.5	10.7	7.0	-2.4	0.74	-0.05	0.56	0.52	1.58	3.40	2.41	1.95
18	GFDL-ESM2M	7.6	12.6	8.9	0.1	0.74	0.02	0.64	0.54	1.75	3.92	2.60	2.13
19	HadGEM2-CC	-29.4	-16.6	-34.1	-39.3	0.76	0.03	0.59	0.45	3.37	4.57	5.25	5.19
20	HadGEM2-ES	-26.9	-14.2	-30.9	-37.5	0.77	0.10	0.63	0.41	3.12	3.95	4.83	4.92
21	INMCM4.0	-56.0	-15.5	-79.0	-78.5	0.64	-0.23	0.61	0.31	6.85	5.36	11.62	10.50
22	IPSL-CM5A-LR	-35.3	-15.5	-44.7	-48.2	0.75	-0.13	0.73	0.55	4.07	4.67	6.54	6.32
23	IPSL-CM5A-MR	-24.7	-14.0	-28.0	-33.6	0.78	0.18	0.61	0.56	2.87	3.93	4.30	4.59
24	MIROC5	-2.0	1.6	-2.8	-5.3	0.79	0.19	0.57	0.52	0.83	1.34	1.16	1.35
25	MIROC5-ESM	-12.1	-11.7	-7.9	-17.2	0.78	0.39	0.65	0.59	1.54	3.20	1.83	2.47
26	MIROC5-ESM-CHEM	-11.8	-11.3	-7.9	-16.6	0.76	0.21	0.66	0.56	1.54	3.17	1.88	2.42
27	MPI-ESM-LR	-35.3	-15.5	-44.7	-48.2	0.75	-0.13	0.73	0.55	4.07	4.67	6.54	6.32
28	MPI-ESM-MR	-24.7	-14.0	-28.0	-33.6	0.78	0.18	0.61	0.56	2.87	3.93	4.30	4.59
29	MRI-CGCM3	-7.1	5.4	-10.5	-18.4	0.79	-0.20	0.66	0.61	1.70	2.49	2.41	2.78
30	NorESM1-M	-16.9	-13.9	-15.9	-21.5	0.74	0.08	0.57	0.41	2.00	3.81	2.68	3.08
31	MME	-16.1	-6.0	-18.9	-25.1	0.83	0.11	0.70	0.61	2.03	1.94	3.05	3.44

Note: Blue font color – represents values for the best models, red font color – denotes values for the worst models and black font color – indicates values between the best and worst models.

Table B2
PBIAS, r and RSR between observed and historical GCM simulations for annual and seasonal T_{max} over the MASB based on MTS data (1981–2005)

No	GCMs	PBIAS				R				RSR			
		Annual	JJAS	FMAM	ONDJ	Annual	JJAS	FMAM	ONDJ	Annual	JJAS	FMAM	ONDJ
1	ACCESS1.0	-18.9	-22.7	-15.1	-18.9	0.56	0.75	0.13	0.18	3.34	6.15	3.75	5.59
2	ACCESS1.3	-23.0	-23.3	-20.1	-25.9	0.77	0.66	0.52	0.47	3.94	6.26	4.78	7.53
3	BCC-CSM1.1(m)	-12.9	-9.1	-13.2	-16.9	0.77	0.45	0.50	0.60	2.41	2.80	3.34	5.08
4	BCC-CSM1.1	-19.7	-26.5	-16.4	-15.7	0.14	0.13	0.03	0.34	3.57	7.17	4.10	4.72
5	BNU-ESM	-18.5	-23.2	-13.4	-18.7	0.57	0.52	0.53	0.34	3.27	6.28	3.25	5.56
6	CanESM2	-3.9	-10.5	-0.6	-0.3	0.35	0.42	0.28	0.52	1.52	3.47	1.53	1.24
7	CCSM4	-24.1	-25.0	-18.6	-29.2	0.74	0.48	0.51	0.57	4.20	6.78	4.52	8.52
8	CESM1-BGC	-23.1	-24.6	-17.3	-27.7	0.74	0.60	0.53	0.53	4.02	6.64	4.20	8.13
9	CESM1-CAM5	-25.6	-30.6	-19.5	-26.8	0.49	0.43	0.17	0.40	4.45	8.19	4.71	7.81
10	CMCC-CM	-10.6	-4.1	-12.8	-15.3	0.79	0.60	0.59	0.59	2.07	1.40	3.17	4.60
11	CMCC-CMS	-12.8	-8.8	-13.5	-16.3	0.82	0.66	0.59	0.52	2.30	2.55	3.27	4.85
12	CNRM-CM5	-1.0	-1.9	2.6	-4.0	0.77	0.57	0.50	0.52	0.93	1.30	1.30	1.77
13	CSIRO-Mk3-6-0	-12.4	-5.3	-15.3	-17.1	0.68	-0.05	0.46	0.49	2.45	1.98	3.75	5.29
14	EC-EARTH	-22.8	-25.1	-21.7	-21.6	0.55	0.57	0.25	0.63	3.96	6.78	5.25	6.30
15	FGOALS-g2	-27.3	-35.3	-22.2	-23.9	0.19	0.53	0.06	0.39	4.77	9.45	5.29	6.95
16	GFDL-CM3	-17.3	-15.3	-13.5	-23.8	0.78	0.64	0.46	0.35	3.13	4.33	3.39	7.06
17	GFDL-ESM2G	-19.4	-18.8	-15.3	-24.7	0.70	0.14	0.42	0.45	3.46	5.24	3.78	7.34
18	GFDL-ESM2M	-18.3	-17.4	-14.5	-23.5	0.67	0.16	0.35	0.37	3.31	4.89	3.67	7.09
19	HadGEM2-CC	-19.8	-24.5	-15.0	-19.9	0.52	0.64	0.11	0.39	3.50	6.64	3.72	5.84
20	HadGEM2-ES	-19.0	-24.1	-14.2	-18.6	0.49	0.63	0.19	0.28	3.38	6.55	3.52	5.46
21	INMCM4.0	-17.9	-19.1	-12.8	-22.2	0.68	0.35	0.51	0.27	3.21	5.36	3.19	6.56
22	IPSL-CM5A-LR	-14.0	-7.5	-15.3	-19.5	0.78	0.20	0.61	0.60	2.58	2.26	3.71	5.79
23	IPSL-CM5A-MR	-14.9	-11.1	-15.6	-18.3	0.76	0.32	0.54	0.51	2.65	3.16	3.75	5.46
24	MIROC5	-18.1	-17.1	-19.4	-17.7	0.64	0.41	0.46	0.45	3.17	4.74	4.61	5.34
25	MIROC5-ESM	-28.1	-32.5	-20.2	-32.1	0.62	0.63	0.42	0.42	4.87	8.70	4.79	9.31
26	MIROC5-ESM-CHEM	-27.9	-32.5	-19.7	-31.8	0.57	0.53	0.33	0.31	4.86	8.72	4.73	9.26
27	MPI-ESM-LR	-14.9	-12.5	-14.5	-18.1	0.75	0.29	0.51	0.49	2.67	3.58	3.58	5.39
28	MPI-ESM-MR	-16.6	-15.2	-16.1	-18.8	0.74	0.24	0.53	0.49	2.92	4.24	3.87	5.60
29	MRI-CGCM3	-8.0	-0.1	-9.5	-15.2	0.70	0.11	0.32	0.43	1.96	1.48	2.67	4.69
30	NorESM1-M	-29.1	-34.8	-22.3	-30.3	0.49	0.29	0.48	0.41	5.02	9.32	5.23	8.78
31	MME	-18.0	-18.6	-15.2	-20.4	0.83	0.70	0.59	0.62	3.08	5.00	3.60	5.94

Note: Blue font color – represents values for the best models, red font color – denotes values for the worst models and black font color – indicates values between the best and worst models.

Appendix C

Table C1
Summary of aggregated ranks and overall aggregated ranks of GCMs for Pr, T_{min} and T_{max} over the four temporal scales in the MASB based on MTS data

No	GCMs	Pr						T_{min}						T_{max}					
		Annual	JJAS	FMAM	ONDJ	∑Agg. Rank	Overall Agg. Rank	Annual	JJAS	FMAM	ONDJ	∑Agg. Rank	Overall Agg. Rank	Annual	JJAS	FMAM	ONDJ	∑Agg. Rank	Overall Agg. Rank
		Agg. Rank	Agg. Rank	Agg. Rank	Agg. Rank			Agg. Rank	Agg. Rank	Agg. Rank	Agg. Rank			Agg. Rank	Agg. Rank	Agg. Rank	Agg. Rank		
1	ACCESS1.0	14	12	3	6	35	**7**	21	23	21	20	85	**22**	19	15	24	18	76	**19**
2	ACCESS1.3	11	21	16	6	54	**12**	12	6	16	12	46	**10**	21	16	20	25	82	**21**
3	BCC-CSM1.1(m)	7	7	13	1	28	**4**	4	1	10	7	22	**3**	6	5	9	5	25	**6**
4	BCC-CSM1.1	19	12	15	16	62	**16**	2	10	1	1	14	**2**	24	28	28	8	88	**23**
5	BNU-ESM	16	26	18	4	64	**17**	7	3	7	8	25	**5**	17	21	5	15	58	**14**
6	CanESM2	7	2	7	11	27	**3**	27	16	27	29	99	**25**	3	7	3	1	14	**3**
7	CCSM4	17	17	24	29	87	**25**	18	5	20	15	58	**17**	24	25	18	28	95	**26**
8	CESM1-BGC	13	21	20	23	77	**20**	13	2	18	14	47	**11**	23	23	16	26	88	**23**
9	CESM1-CAM5	22	25	11	27	85	**21**	15	15	17	18	65	**18**	27	26	28	27	108	**28**
10	CMCC-CM	24	23	12	2	61	**14**	4	26	2	5	37	**8**	4	2	2	3	11	**2**
11	CMCC-CMS	9	9	16	14	48	**9**	2	12	4	6	24	**4**	5	3	3	5	16	**4**
12	CNRM-CM5	12	4	20	13	49	**10**	30	31	28	30	119	**30**	1	1	1	2	5	**1**
13	CSIRO-Mk3-6-0	23	16	7	15	61	**14**	21	14	22	21	78	**21**	7	8	15	7	37	**8**
14	EC-EARTH	5	5	3	20	33	**6**	13	6	13	17	49	**12**	24	24	28	17	93	**25**
15	FGOALS-g2	26	31	1	9	67	**18**	17	20	8	10	55	**15**	30	30	31	20	111	**29**
16	GFDL-CM3	10	8	22	17	57	**13**	15	6	13	22	56	**16**	13	10	13	24	60	**16**
17	GFDL-ESM2G	20	20	27	19	86	**24**	6	20	9	3	38	**9**	18	22	17	22	79	**20**
18	GFDL-ESM2M	21	18	27	27	93	**28**	10	25	11	3	49	**12**	16	18	19	22	75	**17**
19	HadGEM2-CC	4	11	10	6	31	**5**	26	27	26	26	105	**27**	21	20	26	18	85	**22**
20	HadGEM2-ES	3	10	22	10	45	**8**	25	24	25	25	99	**25**	20	18	22	15	75	**17**
21	INMCM4.0	5	14	30	24	73	**19**	31	30	31	31	123	**31**	14	16	5	21	56	**13**
22	IPSL-CM5A-LR	31	27	31	21	110	**31**	28	28	29	27	112	**28**	7	6	7	12	32	**7**
23	IPSL-CM5A-MR	25	19	29	21	94	**29**	23	17	23	23	86	**23**	9	9	10	9	37	**8**
24	MIROC5	30	14	26	31	101	**30**	1	4	2	2	9	**1**	14	14	20	11	59	**15**
25	MIROC5-ESM	28	29	5	25	87	**25**	10	10	4	10	34	**6**	28	26	23	30	107	**27**
26	MIROC5-ESM-CHEM	27	30	2	26	85	**21**	9	13	6	8	36	**7**	29	29	26	31	115	**31**
27	MPI-ESM-LR	15	5	14	18	52	**11**	28	28	29	27	112	**28**	10	11	10	9	40	**10**
28	MPI-ESM-MR	2	1	5	12	20	**2**	23	17	23	23	86	**23**	11	13	14	14	52	**12**
29	MRI-CGCM3	29	28	25	3	85	**21**	8	19	12	12	51	**14**	2	3	10	4	19	**5**
30	NorESM1-M	18	24	19	30	91	**27**	19	22	15	16	72	**20**	30	31	24	29	114	**30**
31	MME	1	3	9	5	18	**1**	19	9	18	19	65	**18**	12	12	7	13	44	**11**

Note: Blue font color – represents overall aggregated ranks for best models and red font color – denotes ranks for worst models.

References

[1] A. Busuioc, D. Chen, C. Hellström, Performance of statistical downscaling models in GCM validation and regional climate change estimates: application for Swedish precipitation, Int. J. Climatol. 21 (2001) 557–578.

[2] R. Yunfeng, Z. Yao, R. Wang, Z. Liu, Ranking of CMIP5 GCM skills in simulating observed precipitation over the Lower Mekong Basin, using an improved score-based method, Wat 10 (2018) 1868. https://doi:10.3390/w10121868.

[3] K. Ahmed, S. Shahid, E.S. Chung, X.J. Wang, S.B. Harun, Climate change uncertainties in seasonal Drought Severity-Area-Frequency curves: case of arid region of Pakistan, J. Hydrol. 570 (2019) 473–485, https://doi.org/10.1016/j.jhydrol.2019.01.019.

[4] Z. Wu, X. Chen, G. Lu, H. Xiao, H. He, J. Zhang, Regional response of runoff in CMIP5 multi-model climate projections of Jiangsu Province, China, Stoch. Environ. Res. Risk Assess. 31 (2016) 2627–2643.

[5] S.E. Perkins-Kirkpatrick, P.B. Gibson, Changes in regional heat wave characteristics as a function of increasing global temperature, Sci. Rep. UK 7 (2017), 12256, https://doi.org/10.1038/s41598-017-12520-2.

[6] Y. Wang, L. Shi, A. Zanobetti, J.D. Schwartz, Estimating and projecting the effect of cold waves on mortality in 209 US cities, Environ. Int. 94 (2016) 141–149.

[7] Y. Xu, C.H. Xu, X.J. Gao, Y. Luo, Projected changes in temperature and precipitation extremes over the Yangtze River basin of China in the 21st century, Quat. Int. 208 (2009) 44–52.

[8] K.V. Ramesh, P. Goswami, Assessing reliability of regional climate projections: the case of Indian monsoon, Sci. Rep. 4 (2014) 4071.

[9] R.K. Srinivasa, K.D. Nagesh, Ranking general circulation models for India using TOPSIS, J. Wat. Clim. Cha. (2014), https://doi.org/10.2166/wcc.2014.074.

[10] P. Pragya, S. Sangam, S.S. Mohana, G.P.V. Salvatore, Evaluation of the CMIP5 general circulation models for simulating the precipitation and temperature of the Koshi River Basin in Nepal, J. Wat.Clim. Cha. 12 (7) (2021) 3282, https://doi.org/10.2166/wcc.2021.124.

[11] S.H. Pour, S. Shahid, E.S. Chung, X.J. Wang, Model output statistics downscaling using support vector machine for the projection of spatial and temporal changes in rainfall of Bangladesh, Atmos. Res. 213 (2018) 149–162, https://doi.org/10.1016/j.atmosres.2018.06.006.

[12] R.L. Wilby, I. Harris, A framework for assessing uncertainties in climate change impacts: low flow scenarios for the river Thames, UK, Wat. Resour. Res. 42 (2006), W02419.

[13] S.K. Thair, A.A. Imzahim, M.H. Ali, Selection of suitable precipitation CMIP5 sets of GCMs for Iraq using a symmetrical uncertainty filter, IOP Conf. Ser. Mater. Sci. Eng. 671 (2020), 012013.

[14] A.F. Lutz, H.W. Ter Maat, H. Biemans, A.B. Shrestha, P. Wester, W.W. Immerzeel, Selecting representative climate models for climate change impact studies: an advanced envelope-based selection approach, Int. J. Climatol. 36 (2016) 3988–4005.

[15] K.E. [Taylor, R.J. Stouffer, G.A. Meehl, An overview of CMIP5 and the experiment design, B. Am. Meteorol. Soc. 93 (2012) 485–498.

[16] Y. Gao, H. Wang, D. Jiang, An intercomparison of CMIP5 and CMIP3 models for interannual variability of summer precipitation in Pan-Asian monsoon region, Int. J. Climatol. 35 (2015) 3770–3780.

[17] S. Kusunoki, O. Arakawa, Are CMIP5 models better than CMIP3 models in simulating precipitation over East Asia? J. Clim. 28 (2015) 5601–5621, https://doi.org/10.1175/JCLI-D-14-00585.1.

[18] C. Onyutha, A. Rutkowska, P. Nyeko-Ogiramoi, P. Willems, How well do climate models reproduce variability in observed rainfall? A case study of the Lake Victoria basin considering CMIP3, CMIP5 and CORDEX simulations, Stoch. Environ. Res. Risk Assess. 33 (2019) 687–707, https://doi.org/10.1007/s00477-018-1611-4.

[19] C. Onyutha, H. Tabari, A. Rutkowska, P. Nyeko-Ogiramoi, P. Willems, Comparison of different statistical downscaling methods for climate change rainfall projections over the Lake Victoria basin considering CMIP3 and CMIP5, J. Hydro-environ. Res. 12 (2016) 31–45. https://doi:10.1016/j.jher.2016.03.001.

[20] K. Hayhoe, J. Edmonds, R. Kopp, A. LeGrande, B. Sanderson, M. Wehner, D. Wuebbles, Climate Models, Scenarios, and Projections, US Glo. Cha. Res. Prog., Washington, D.C., USA, 2017, pp. 133–160, https://doi.org/10.7930/J0WH2N54.

[21] N. Herger, G. Abramowitz, R. Knutti, O. Angélil, K. Lehmann, B.M. Sanderson, Selecting a climate model subset to optimize key ensemble properties, Ear. Syst. Dynam. 9 (2018) 135–151, https://doi.org/10.5194/esd-9-135-2018.

[22] Z. Sa'adi, M.S. Shiru, S. Shahid, T. Ismail, Selection of general circulation models for the projections of spatiotemporal changes in temperature of Borneo Island based on CMIP5, Theor. Appl. Climatol. (2019), https://doi.org/10.1007/s00704-019-02948-z.

[23] M.S. Shiru, S. Shahid, E.S. Chung, N. Alias, L. Scherer, A MCDM-based framework for selection of general circulation models and projection of spatio-temporal rainfall changes: a case study of Nigeria, Atmos. Res. 225 (2019) 1–16. https://doi:10.1016/j.atmosres.2019.03.033.

[24] S.A. Salman, S. Shahid, T. Ismail, K. Ahmed, X.J. Wang, Selection of climate models for projection of spatiotemporal changes in temperature of Iraq with uncertainties, Atmos. Res. 213 (2018) 509–522. https://doi:10.1016/j.atmosres.2018.07.008.

[25] R. Seager, M. Ting, I. Held, Y. Kushnir, J. Lu, G. Vecchi, H.P. Huang, N. Harnik, A. Leetmaa, N.C. Lau, Model projections of an imminent transition to a more arid climate in Southwestern North America, Science 316 (2007) 1181–1184.

[26] D.W. Pierce, T.P. Barnett, B.D. Santer, P.J. Gleckler, Selecting global climate models for regional climate change studies, Proc. Nat. Aca. Sci. 106 (21) (2009) 8441–8446. https://doi:10.1073/pnas.0900094106.

[27] H. Biemans, L. Speelman, F. Ludwig, E. Moors, A. Wiltshire, P. Kumar, D. Gerten, P. Kabat, Future water resources for food production in five South Asian river basins and potential for adaptation – a modeling study, Sci. Total Environ. 468 (2013) S117–S131.

[28] A.F. Lutz, W.W. Immerzeel, H. Biemans, H. ter Maat, V. Veldore, A. Shrestha, Selection of Climate Models for Developing Representative Climate Projections for the Hindu Kush Himalayan Region, Hi-Aware, 2016, p. 46, available from: http://lib.icimod.org/record/31874/files/HI-AWARE-WP1.pdf.

[29] I. Hassan, R.M. Kalin, C.J. White, J.A. Aladejana, Selection of CMIP5 GCM ensemble for the projection of spatiotemporal changes in precipitation and temperature over the Niger Delta, Nigeria, Wat 12 (2020) 1–19.

[30] S. Arpit, D.K. Ganesh, Ranking of general circulation models for Surat City by using a hybrid approach, Wat. Prac. Techno. 17 (10) (2022), 2186, https://doi.org/10.2166/wpt.2022.118.

[31] R. Homsi, M.S. Shiru, S. Shahid, T. Ismail, S.B. Harun, N. Al-ansari, K. Chau, Z. Mundher, Precipitation projection using a CMIP5 GCM ensemble model: a regional investigation of Syria, Eng. App.Comput. Flu. Mec. (2020), https://doi.org/10.1080/19942060.2019.1683076.

[32] A.R. Mahmoud, M. Hassan, M. Hany, A. Mostafa, Multi criterion decision making techniques for ranking regional climate models over Wadi El-Natrun catchment, Aus. J. Bas. App. Sci. 13 (5) (2019) 85–96, https://doi.org/10.22587/ajbas.2019.13.5.9.

[33] A. Jacob, A. Thompson, L. Benjamin, Q. Emmannuel, Y.K.A. Richard, Evaluation of CMIP5 global climate models over the Volta basin: precipitation, 2018, Adv. Meteor. (2018), 4853681, https://doi.org/10.1155/2018/4853681, 24.

[34] Z. Sinclaire, J. Shipra, S. Popat, S. Shayan, K.M. Saroj, Assessment of CMIP5 multimodel mean for the historical climate of Africa, Atmos. Sci. Lett. 20 (2019) e926, https://doi.org/10.1002/asl.926.

[35] N.R. Hounguè, A.D.S. Almoradie, M.A. Evers, Multi criteria decision analysis approach for regional climate model selection and future climate assessment in the Mono River Basin, Benin and Togo, Atmos 13 (2022) 1471, https://doi.org/10.3390/atmos13091471.

[36] C. Onyutha, Analyses of rainfall extremes in East Africa based on observations from rain gauges and climate change simulations by CORDEX RCMs, Clim. Dynam. 54 (2020) 4841–4864, https://doi.org/10.1007/s00382-020-05264-9.

[37] B. Ayugi, G. Tan, G.G. Tchalim, M. Ojara, V. Ongoma, Historical evaluations and simulations of precipitation over East Africa from Rossby centre regional climate model, Atmos. Res. 232 (2020), 104705, https://doi.org/10.1016/j.atmosres.2019.104705.

[38] O.M. Ogega, J. Koske, J.B. Kung`u, E. Scoccimarro, H.S. Endris, M.N. Mistry, Heavy precipitation events over East Africa in a changing climate: results from CORDEX RCMs, Clim. Dynam. 55 (2020) 993–1009, https://doi.org/10.1007/s00382-020-05309-z.

[39] S.M. Yimer, A. Bouanani, N. Kumar, B. Tischbein, C. Borgemeister, Assessment of climate models performance and associated uncertainties in rainfall projection from CORDEX over the Eastern Nile Basin, Ethiopia, Clim. Past 10 (2022) 95, https://doi.org/10.3390/cli10070095.

[40] A.S. Bokke, M.T. Taye, P. Willems, S.A. Siyoum, Validation of general climate models (GCMs) over upper blue nile River Basin, Ethiopia, Atmos. Clim. Sci. 7 (2017) 65–75, https://doi.org/10.4236/acs.2017.71006.

[41] D. Ellen, W. Richard, T.T. Meron, Evaluating the CMIP5 ensemble in Ethiopia: creating a reduced ensemble for rainfall and temperature in Northwest Ethiopia and the Awash basin, Int. J. Climatol. (2019) 1–22, https://doi.org/10.1002/joc.6377.

[42] R.J. Mark, Statistical evaluation of CMIP5 climate change model simulations for the Ethiopian highlands, Int. J. Climatol. 35 (2015) 37–44, https://doi.org/10.1002/joc.3960.

[43] S.B. Partha, F.Z. Benjamin, Perspectives on CMIP5 model performance in the Nile River headwaters regions, Int. J. Climatol. 35 (2015) 4262–4275, https://doi.org/10.1002/joc.4284.

[44] V. Ongoma, C. Haishan, G. Chujie, Valuation of CMIP5 twentieth century rainfall simulation over the equatorial East Africa, Theor. Appl. Climatol. (2019), https://doi.org/10.1007/s00704-018-2392-x.

[45] R. Girma, C. Fürst, A. Moges, Performance evaluation of CORDEX-Africa regional climate models in simulating climate variables over Ethiopian main rift valley: evidence from Gidabo river basin for impact modeling studies, Dynam. Atmos. Oceans 99 (2022), 101317, https://doi.org/10.1016/j.dynatmoce.2022.101317.

[46] T.D. Geleta, D.K. Dadi, C. Funk, W. Garedew, D. Eyelade, A. Worku, Downscaled climate change projections in urban centers of Southwest Ethiopia using CORDEX Africa simulations, Clim. Past 10 (2022) 158, https://doi.org/10.3390/cli10100158.

[47] M. Almazroui, M.N. Islam, S. Saeed, A.K. Alkhalaf, R. Dambul, Assessment of uncertainties in projected temperature and precipitation over the Arabian Peninsula using three categories of CMIP5 multimodel ensembles, Ear. Syst. Environ. 1 (23) (2017) 1–20. https://doi:10.1007/s41748-017-0027-5.

[48] C.Y. Miao, Q.Y. Duan, Q.H. Sun, Y. Huang, D.X. Kong, T.T. Yang, A.Z. Ye, Z.H. Di, W. Gong, Assessment of CMIP5 climate models and projected temperature changes over Northern Eurasia, Environ. Res. Lett. 9 (2014), 055007.

[49] S. Kumar, V. Merwade, J.L. Kinter III, D. Niyogi, Evaluation of temperature and precipitation trends and long-term persistence in CMIP5 twentieth-century climate simulations, J. Clim. 26 (2013) 4168–4185.

[50] O. Penalba, J. Rivera, Regional aspects of future precipitation and meteorological drought characteristics over southern South America projected by a CMIP5 multimodel ensemble, Int. J. Climatol. 36 (2016) 974–986.

[51] K.V. Ramesh, P. Goswami, Assessing reliability of regional climate projections: the case of Indian monsoon, Sci. Rep. 4 (2014) 4071.

[52] M. Abbasian, S. Moghim, A. Abrishamchi, Performance of the general circulation models in simulating temperature and precipitation over Iran, Theor. Appl. Climatol. 135 (2019) 1465–1483. https://doi.org/10.1007/s00704-018-2456-y.

[53] K.N. Tufa, Review on status, opportunities and challenges of irrigation practices in Awash River Basin, Ethiopia, Agrotech 10 (4) (2021) 207. https://doi:10.35248/2168-9881.21.10.207.

[54] N. Kebede, Awash River's the ongoing irrigation practices, future projects and its impacts on the environment of Awash River Basin, Irrigat. Drainage. Sys. Eng. 10 (6) (2021) 272.

[55] Y. Getahun, S. Gebre, Flood hazard assessment and mapping of flood inundation area of the Awash River Basin in Ethiopia using GIS and HEC-GeoRAS/HEC-RAS Model, J. Civ. Environ. Eng. 5 (2015) 179.

[56] A. Zekarias, T. Yosef, B. Asmrom, F. Elias, Guideline and standardized operational procedure on data blending and integration for NMA merged dataset, Nat. Meteor. Age., Addis Ababa, Ethiopia (2018) 1–31.

[57] K. Taylor, R. Stouffer, G. Meehl, An overview of CMIP5 and the experiment design, Bul. Am. Meteorol. Soc. 93 (4) (2012) 485–498, https://doi.org/10.1175/BAMS-D-11-00094.

[58] Huang S., Wang Y., Xie Y., Zhao P., Lüers J., OutlierFlag: a tool for scientific data quality control by outlier data flagging, J. Ope. Res. Soft. 4 (2016) e20, https://doi:10.5334/jors.90.

[59] XLSTAT by Addinsoft, Statistical and Data Analysis Solution Version 2018.7.5, Addinsoft, Paris, France, 2018. https://www.xlstat.com.

[60] P. Stepanek, AnClim - Software for time series analysis, Depar. Geog. Carto., Fac. Sci., Masaryk Uni., Brno, Czech Republic. 1 (2008). https://www.climahom.eu.

[61] A. Theissen, Precipitation averages for large areas, Mon. Weather Rev. 39 (1911) 1082–1084.

[62] W. Gebrekidan, T. Ermias, B. Amare, T.D. Yihun, T.T. Meron, Evaluation of regional climate models performance in simulating rainfall climatology of Jemma sub-basin, Upper Blue Nile Basin, Ethiopia, Dynam. Atmos. Oceans 83 (2018) 53–63, https://doi.org/10.1016/j.dynatmoce.2018.06.002.

[63] A.A. Mekonen, A.B. Berlie, Spatiotemporal variability and trends of rainfall and temperature in the northeastern highlands of Ethiopia, Mod. Earth Syst. Environ. 6 (2019) 285–300.
[64] R.K. Srinivasa, K.D. Nagesh, Multicriterion Analysis in Engineering and Management, PHI Learn. Pri. Lim., New Delhi, India, 2014.
[65] J.Ch Pomerol, S.B. Romero, Multicriterion Decision in Management: Principles and Practices, Kluwer Aca., Netherlands, 2000.
[66] H.S. Shih, H.J. Shyur, E.S. Lee, An extension of TOPSIS for group decision making, Math. Comput. Model. 45 (2007) 801–813.
[67] W. Wang, N. Fenton, Risk and Confidence Analysis for Fuzzy Multicriteria Decision-Making, 2007 (technical report is available at: www.dcs.qmul.ac.uk/~norman/papers/Wang Fenton Risk and Confidence.pdf.
[68] R.A. Aomar, in: E. Yucesan, C.H. Chen, J.L. Snowdon, J.M. Charnes (Eds.), A Robust Simulation-Based Multicriteria Optimization Methodology, Proceedings of the 2002 Winter Simulation Conference, Inst. Elect. Electro. Eng., San Diego, CA, 2002, pp. 1931–1939. https://www.informs-cs.org/wsc02papers/267.pdf.
[69] C. Hwang, K. Yoon, Multiple Attribute Decision Making, Methods and Applications, a State-Of-The-Art Survey, Springer-Verlag, 1981.
[70] T.L. Satty, How to make a decision: the analytic Hierarchy process, Eur. J. Oper. Res. 48 (1990) 9–26.
[71] D.Y. Chang, Applications of the extent analysis method on fuzzy AHP, Eur. J. Oper. Res. 93 (1996) 633–649.
[72] A. Shanian, O. Savadogo, Using multi-pseudo criteria and fuzzy outranking relation analysis for material selection of bipolar plates for PEFCs, J. Electrochem. Soc. 133 (3) (2006) A887–A896.
[73] L. Duckstein, A. Tecle, H.P. Nachnebel, B.F. Hobbs, Multicriterion analysis of hydropower operation, J. Ene. Eng. 115 (3) (1989) 132–153.
[74] A. Goicoechea, D. Hansen, L. Duckstein, Introduction to Multiobjective Analysis with Engineering and Business Applications, John Wiley, New York, USA, 1982.
[75] F. Szidarovszky, M. Gershon, L. Duckstein, Techniques for Multiobjective Decision Making in Systems Management, Elsevier, Amsterdam, Netherlands, 1986.
[76] L. Duckstein, W. Treichel, S.E. Magnouni, Ranking groundwater management alternatives by multicriterion analysis, J. Wat. Resou. Plan. Manag. ASCE 120 (4) (1994) 546–565.
[77] A.T. Hordofa, O.T. Leta, T. Alamirew, A.D. Chukalla, Spatiotemporal trend analysis of temperature and rainfall over Ziway Lake basin, Ethiopia, Hydro 9 (2022) 2, https://doi.org/10.3390/hydrology9010002.
[78] K. Kiya, M. Boja, R. Negese, Evaluation of the performance of regional climate models in simulating rainfall characteristics over Upper Awash Sub-basin, Ethiopia, Intern. Res. Jou. Adv. Eng. Sci. 5 (1) (2020) 134–138.
[79] K. Ahmed, D.A. Sachindra, S. Shahid, M.C. Demirel, E.S. Chung, Selection of multi-model ensemble of general circulation models for the simulation of precipitation and maximum and minimum temperature based on spatial assessment metrics, Hydrol. Ear. Syst. Sci. 23 (2019) 4803–4824, https://doi.org/10.5194/hess-23-4803-2019.
[80] Deepthi, B., and Ashwini, B.M. Ranking of CMIP5 Climate Models for Statistical Downscaling for Upper Godavari River Basin. [Unpublished paper].
[81] P. Pradhan, S. Shrestha, S.M. Sundaram, S.G.P. Virdis, Evaluation of the CMIP5 general circulation models for simulating the precipitation and temperature of the Koshi River Basin in Nepal, J. Wat. Clim. Chan. 12 (7) (2021) 3282. https://doi:10.2166/wcc.2021.124.
[82] E. Dyer, R. Washington, T.M. Teferi, Evaluating the CMIP5 ensemble in Ethiopia: creating a reduced ensemble for rainfall and temperature in Northwest Ethiopia and the Awash basin, Int. J. Climatol. (2019) 1–22, https://doi.org/10.1002/joc.6377.
[83] A. Sharma, G.D. Kale, Ranking of general circulation models for Surat City by using a hybrid approach, Water Pract. Technol. 17 (10) (2022) 2186. https://doi:10.2166/wpt.2022.118.
[84] Dataset: ASF DAAC, ALOS PALSAR_Radiometric_Terrain_Corrected_High_Resolution, in: Includes Material © JAXA/METI 2007, Accessed through ASF DAAC, 2015, https://doi.org/10.5067/Z97HFCNKR6VA. https://search.asf.alaska.edu/. (Accessed 1 June 2022).